Efficient Strategies for Modeling Polarons using Density Functional Theory

A major Qualifying Project Report

Submitted to the Faculty of the

Worcester Polytechnic Institute

in partial fulfillment of the requirements for the

Degree of Bachelor of Science in

Chemical Engineering

by

Thang Duc Pham

Date: April 25th, 2019

Advisor: Professor N. Aaron Deskins

Efficient Strategies for Modeling Polarons using Density Functional Theory

Thang Duc Pham and N. Aaron Deskins*

Department of Chemical Engineering, Worcester Polytechnic Institute, Worcester, MA

E-mail: nadeskins@wpi.edu

1 Introduction

The understanding of materials brings about the assessment of their new potential applications and the development of novel materials. Semiconductor, an important class material thanks to its peculiar electronic structure, has attracted a major fraction of modern scientific research. A wide range of semiconductors have been discovered and used extensively in the fabrication of electronic devices[1–3] and light-harvesting applications, specifically photovoltaics[4–9] and photocatalysis.[10–12] A comprehensive understanding of semiconductor properties is thus necessary to further enhance its efficiency as well as to explore novel and potential semiconductors for these applications.

Metal oxide semiconductors are promising candidates for the above-mentioned applications because of their stability and their relative abundance. However, they often suffer from poor charge transport properties, which is important for the semiconductor efficiency. For instance, in photocatalysis, upon the absorption of light, excited electrons and holes are created. If the charge carriers have high mobility, they can quickly diffuse to the surface of the photocatalyst and complete the photocatalytic cycle. In metal oxide, charge carriers are often self-trapped and form a "polaron",[13–16] which involves the self-trapped charge carrier and the lattice distortion created upon self-trapping. The polaron formation greatly limits the charge carrier mobility because polaron transport (or polaron hopping) is a thermally activated process. Although the polaron theory has been proposed for a long time to explain the low mobility of charge carrier in semiconductor, it was not until recently that polaron has been experimentally observed.[17,18] Therefore, theory can play an important role in explaining and predicting polaron formation.

Density functional theory (DFT), a computational quantum mechanical modelling method, has been the major approach for the study of polaron.[19–25] However, many challenges remain in modeling polaron with DFT, including (1) the corrections to overcome the self-interaction error in DFT, such as Hubbard[26–28] correction and hybrid functionals, (2) the degree of corrections being employed and (3) the lack of a consistent procedure to model polaron. Overcoming these problems would allow for a consistence polaron study and a prediction of polaron formation in new materials.

This Major Qualifying Project (MQP) aimed to solve the difficulties of modeling polarons within the DFT framework. By studying electron polaron formation in several transition-metal oxide semiconductors, our goals were to develop a comprehensive strategy for efficient (with respect to speed and accuracy) modeling of polarons.

2 Background

2.1 Uses of Semiconductor Materials

Semiconductors are solid materials that have energy bands, or orbitals, separated by an energy gap. This energy gap, the band gap, is defined as the energy difference between the semiconductor's valance band and conduction band (Figure 1a) This band gap can have important implications on different applications such as in light-harvesting technology, and electronic devices.

In light-harvesting applications, electrons in a semiconductor's valance band are excited

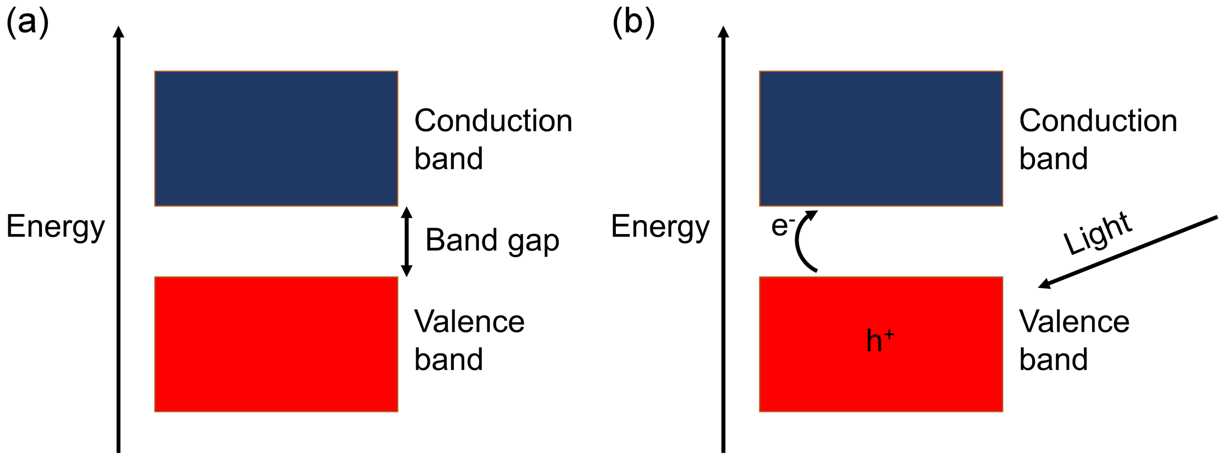

Figure 1: (a) Band structure of a semiconductor, and (b) photoexcited electron in photocatalysis and photovoltaics

to the conduction band (Figure1b). The excited electrons can participate in chemical reaction and convert photon energy into chemical energy through photocatalysis. This excited electrons can also be harvested through an external circuit and used as electrical energy, such as in a photovoltaic device. Many semiconductors have been used to harvest light, such TiO_2,[29] g-C_3N_4,[30] α-Fe_2O_3.[31] In electronic devices, different semiconductors allow control of electrical current flow. Semiconductors play an important role in electronic devices such in diodes[2] and transistors.[3]

Depending on the applications, certain requirements are considered in choosing a semiconductor, such as price and stability under operating conditions. One of the most important characteristic is charge conductivity. Faster charge conductivity can lead to improved efficiency for a semiconductor. For instance, upon absorption of light semiconductors create excited electrons and holes (Figure 1b). If the electrons can quickly get to the surface of the semiconductor before recombining with the holes, they can participate in chemical reactions and reduce reactants during a photocatalytic cycle. On the other hand, if electrons fail to diffuse to the surface, and instead recombine with holes they cannot facilitate the reactions. Therefore, understanding the nature of charge carriers in semiconductors can give insight into improving charge conductivity, their lifetime, and improving the performance of semiconductors.

2.2 Nature of Polarons

Charge conductivity in semiconductors depends on how the charge carriers move through the materials. Two types of charge transport can occur in semiconductors: band-like conduction and polaron hopping. Band-like conduction shares similar characteristics to conduction in metals, in which charge carriers are dispersed across multiple atoms in bands and this results in high charge conductivity. On the contrary, polaron hopping involves self-trapping of the charge carriers, which results in lower charge conductivity. During polaron transport the self-trapped charge hops from one site to another, and must overcome an activation barrier to hop from site to site (Figure 2).

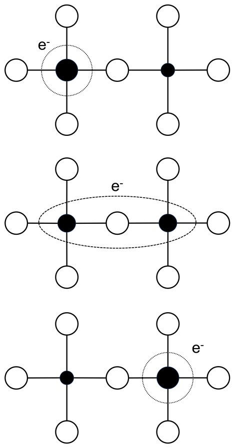

Figure 2: Schematic for polaron hopping process in TiO_2. Black atoms represents Ti and white atoms represent O. Top: electron is localized on the Ti atom on the left. Middle: electron is shared between the two Ti atoms. Bottom: electron hops and is localized on Ti atom on the right. Larger sphere radius indicates the effect of electron being localized on specific atom.

A polaron is a quasiparticle resulting from the interactions of a conducting (or unpaired) electron (or a hole) with vibrating ions. Such interactions create local distortions on surrounding ions, and the potential well produced by these distortions lowers the carrier's energy and confine the carrier on an ion.[16] Depending on its spatial extension, a polaron can be classified as a "large polaron" or a "small polaron". A large polaron involves charge carriers having large spatial extent, typically greater than the bulk lattice cell of the material. In contrast, a "small polaron" is confined to a region smaller than the cell, usually an atom or a few atoms. Instead of going into details about polaron characteristics, we refer the readers to several helpful reviews on polaron.[13–16]

Different types of polaron result in different carrier mobility. Experimentally, the carrier mobility in solid materials is often determined by drift mobility, which measures the mobility caused by an electric field due to an externally applied voltage. Large polarons usually have moderate drift mobility values, which are greater than 1 $cm^2V^{-1}s^{-1}$, such as with SnO_2[16] and WO_3.[32] Small polarons have an extremely small drift mobility value on the order of 10^{-4} -10^{-1} $cm^2V^{-1}s^{-1}$, such as with $BiVO_4$[33] and α-Fe_2O_3.[7]

Several metal oxides are potential semiconductors in the above-mentioned applications because they are stable under aqueous and oxidized environments (the operating conditions for light-harvesting and electronic devices applications, respectively) and they are cheap. However, it has been proposed that the charge transport mechanism in several metal oxides is polaron hopping, which results in low charge conductivity. Therefore, a better understanding of polaron formation could provide a basis to understand charge transport in metal oxides. Prediction of polaron formation especially could help screen new materials for electronic devices, photocatalysis and photovoltaic applications.

2.3 Previous Modeling of Polarons

Several approaches have been employed to model and study polarons in metal oxides. In this section, we give an overview of previous modeling of polaron formation in (1) TiO_2 rutile and anatase, (2) monoclinic $BiVO_4$ (m-$BiVO_4$), and (3) monoclinic HfO_2 (m-HfO_2). These four materials have been used in all main applications of semiconductors. TiO_2 rutile, anatase and m-$BiVO_4$ have been widely used in photocatalytic applications.[34–37] $\alpha-Fe_2O_3$ has been used as photoanode for photovoltaics applications.[38,39] m-HfO_2 has been used widely in electronic devices such as in transistor gate dielectric stack[40,41] and in resistance switching random access memory (RRAM).[42]

Deskins et. al[19] modeled small polarons in the two phases of TiO_2 (rutile and anatase), showing that a small polaron is formed in both phases. They predicted that intrinsic electron transport in bulk titania is faster in rutile than in anatase. Using hybrid density functional theory (DFT), Spreafico et. al[21] also modeled polaron formation in TiO_2 rutile and anatase, showing agreement with Deskins et. al[19] that a small polaron is formed in rutile. However, their results predicted large polaron formation in anatase. Setvin et. al[20] combined both theory and experiments, showing that polaron formation is always favorable in TiO_2 rutile, while for anatase, the polaron type depends on the source of the excess electron, with small polaron formation occurs with a surface O vacancy and large polaron formation occurs with Nb-doped TiO_2.

Ramo et. al[24] modeled electron and hole polarons formation in monoclinic HfO_2 and predicted that both electron and hole polaron formation are favorable in m-HfO_2. Wang et. al[42] experimentally measured charge conductivity in $Pt/HfO_2 - x/TiN$, showing that small polaron hopping accounts for the conductance in low-resistance states of bulk HfO_2. Cheng et al.,[43] using density functional theory, also showed that the excess electrons from oxygen vacancies in bulk HfO_2 form polarons at high vacancy concentration.

Using first principle calculations, Kweon et. al[22] predicted electron polaron formation in m-$BiVO_4$ with a hopping barrier of 0.35 eV. Liu et. al,[44] using first principles and mesoscale kinetic simulations, predicted intrinsic electron and hole polaron transport in m-$BiVO_4$. The results emphasize the importance of facet selectivity in charge carrier mobility. Ziwritsch et. al[18] experimentally observed hole polaron formation in m-$BiVO_4$ and measured the hole mobility and thermal hopping activation energy. Rettie et. al[16] studied the electrical transport properties of single crystal of W and Mo-doped $BiVO_4$, showing that their resistivity data fits the small polaron hopping model.

2.4 Challenges in Modeling Polarons

Molecular modeling at atomic scale can bring important insights as well as predict polaron formation, charge carrier mobility and polaron hopping barrier. Density Functional Theory (DFT), a computational quantum mechanical modelling method, has been used widely for these purposes. A thorough review of DFT will be addressed in the Methodology section.

Although DFT has been used widely to model polaron formation, several intrinsic drawbacks of DFT should be addressed in order to gain confidence over the model results. Firstly, to form a polaron, corrections to the self-interaction error in DFT must be used, either in the form of a Hubbard correction[26–28] or a hybrid functional. Density functional theory with Hubbard correction, or so-called DFT+U, is used to treat strong on-site Coulomb interaction of localized electrons that is not well describe by pure DFT. Hybrid functional is a type of approximation to the exchange-correlation energy of DFT that incorporates a portion of exact exchange from Hartree-Fock theory. These corrections lead the second problem, in which polaron formation depends on the type and the extent of the corrections. For example, polarons can only be formed at certain $U_{effective}$ values[20] with Hubbard correction or at certain percentage Hartree-Fock exchange values.[21,44] As a result, choosing the 'right' correction is important in better modeling of polarons in semiconductors. Thirdly, even with those corrections applied, polarons might form, depending on other simulation parameters, such as the initial geometry. Therefore, having effective techniques to model polarons can greatly improve modeling of polaron formation.

3 Methodology

3.1 Overview of Density Functional Theory

The Schrdinger equation is the fundamental equation of physics for describing quantum mechanical behavior. The time-independent Schrdinger equation is expressed as

$$\hat{H}\psi = E\psi$$

where $\hat{H}$ is the Hamiltonian operator, which corresponds to the sum of the kinetic energies and potential energies of all the particles in the system; E is the energy level of the system and ψ is the wavefunction that defines the state of the system at each spatial position. Solving Schrdinger equation gives the exact wavefunction of the system, from which we can obtain observable quantities. However, the Schrdinger cannot be solved exactly for system than contains more than two electrons. As a result, different approximations are employed to get the approximate solutions for Schrdinger equation such as Hartree Fock theory, perturbation theory and Density Functional Theory (DFT) approach.

Compared to other approximations, DFT gives the best balance between calculation speed and accuracy. As a result, DFT has been a powerful tool to explore and understand the electronic structure of molecules, bulk materials, surfaces and nanoparticles. DFT has been used to understand molecular-level structures,[45,46] catalytic processes,[47] electron transport,[19,20,23] solar energy harvesting and conversion, and many more applications.

DFT is a quantum mechanical approach proposed by Kohn and Sham[48] to approximate the solution for the difficult many-body system in the Schrodinger equation. DFT uses a reference system in which electrons are noninteracting, more specifically, uncorrelated (except that they must obey Pauli exclusion principle), and are assumed to only interact through an effective, average electrostatic potential. An exchange-correlation functional is used to correct for this assumption. As a result, the accuracy of DFT calculations depend on the formulation of the exchange-correlation functional. The most commonly used exchange-correlation functionals in solid-state calculations utilize the generalized gradient approximation (GGA), which use the information about the local electron density and the local gradient in the electron density to calculate the electron exchange and correlation energy. The electron density gives the probability of an electron being at a certain location in space around the nuclei. An example of a GGA functional is the functional proposed by Perdew Burke Ernzerhof (PBE).[49]

Similar to other ab initio methods, DFT uses basis sets to approximate the electronic wavefunction. Depending on the system, a molecular basis sets (such as 6-31G) which uses Gaussian functions to describe the electrons, or a plane wave basis sets, which utilizes periodic boundary conditions, can be used. Different DFT codes have been developed using these different types of basis sets. For example, NWChem and Gaussian are common DFT codes for molecular system, while Vienna Ab initio (VASP), CASTEP and Quantum-Espresso are commonly used for periodic system.

Because DFT includes self-exchange and self-correlation interactions, in which electron can exchange and correlate with itself, DFT tends to produce excessively delocalized charge distributions.[50] This excessive delocalization gives rise to problems such as producing too small a band gap in semiconductors[19,43,44,51] or underestimating the stability of high-spin states solids with high magnetic moments. A correction term for this delocalized behavior, the Hubbard correction or DFT+U[26–28] method, has often been employed to overcome this delocalization problem by including correction factors for the strong on-site Coulomb interaction of localized electrons. Therefore, DFT+U can be used to better model highly localized electrons such as with polaron formation or defects. Another approach to better describe electronic structures is hybrid-GGA, which include a partial or full Hartree-Fock exchange to decrease or eliminate the self-interaction error.

3.2 Computational Details

We summarize our approach to modeling polarons in the following. The reader may read several excellent reviews[30,52,53] to further understand the nature of DFT modeling and the parameters involved.

3.2.1 Modeling Parameters

Spin polarized DFT calculations were performed using the Vienna Ab initio Simulation Package (VASP).[54–57] The valence electrons were represented by plane waves with a cutoff energy of 450 eV for TiO_2 rutile, TiO_2 anatase and 500 eV for monoclinic $BiVO_4$ and 550 eV for monoclinic m-HfO_2, similar to other theoretical work on these materials.[19,22,43,58] Core electrons were treated by projector augmented wave (PAW) potentials.[59,60] The number of valence electrons for O, Ti, Hf, V, Ta, Cr and Bi were 6, 10, 10, 11, 11, 12 and 15, respectively. We used the generalized gradient approximation by Perdew-Becke-Ernzerhof(PBE)[49] for the exchange correlation functional. The convergence criteria for electronic states and geometries were 10^{-5} eV and 2x10^{-2} eV/A, respectively.

For TiO_2 lattice parameter optimization, a k-point mesh of 12x12x12 was used for the unit cell of both rutile and anatase. The optimized lattice parameters were found to be a = 4.65 Å, c = 2.98 Å for rutile, and a = 3.81 Å, c = 9.72 Å for anatase. The calculated lattice parameters are in good agreement with literature.[19,25,61] We modelled supercells of (3x3x3) for rutile, and (3x3x2) for anatase when modeling polarons. Reciprocal space was sampled with k-point meshes of 2x2x2 for rutile and 2x2x1 for anatase, similar to Deskins et. al.[19] The final supercell of rutile (Figure 3a) contain 162 atoms with the size of 13.95 Å x 13.95 Å x 8.93 Å. The supercell of anatase (Figure 3b) contain 216 atoms with the size of 11.43 Å x 11.43 Å x 19.43 Å.

When modeling monoclinic HfO_2, a k-point mesh of 10x10x10 was used to optimize the lattice parameters. The equilibrium volume of m-HfO_2 was obtained by fitting the DFT energies and volumes data with the Murnaghan[62] equation of state. The equilibrium volume

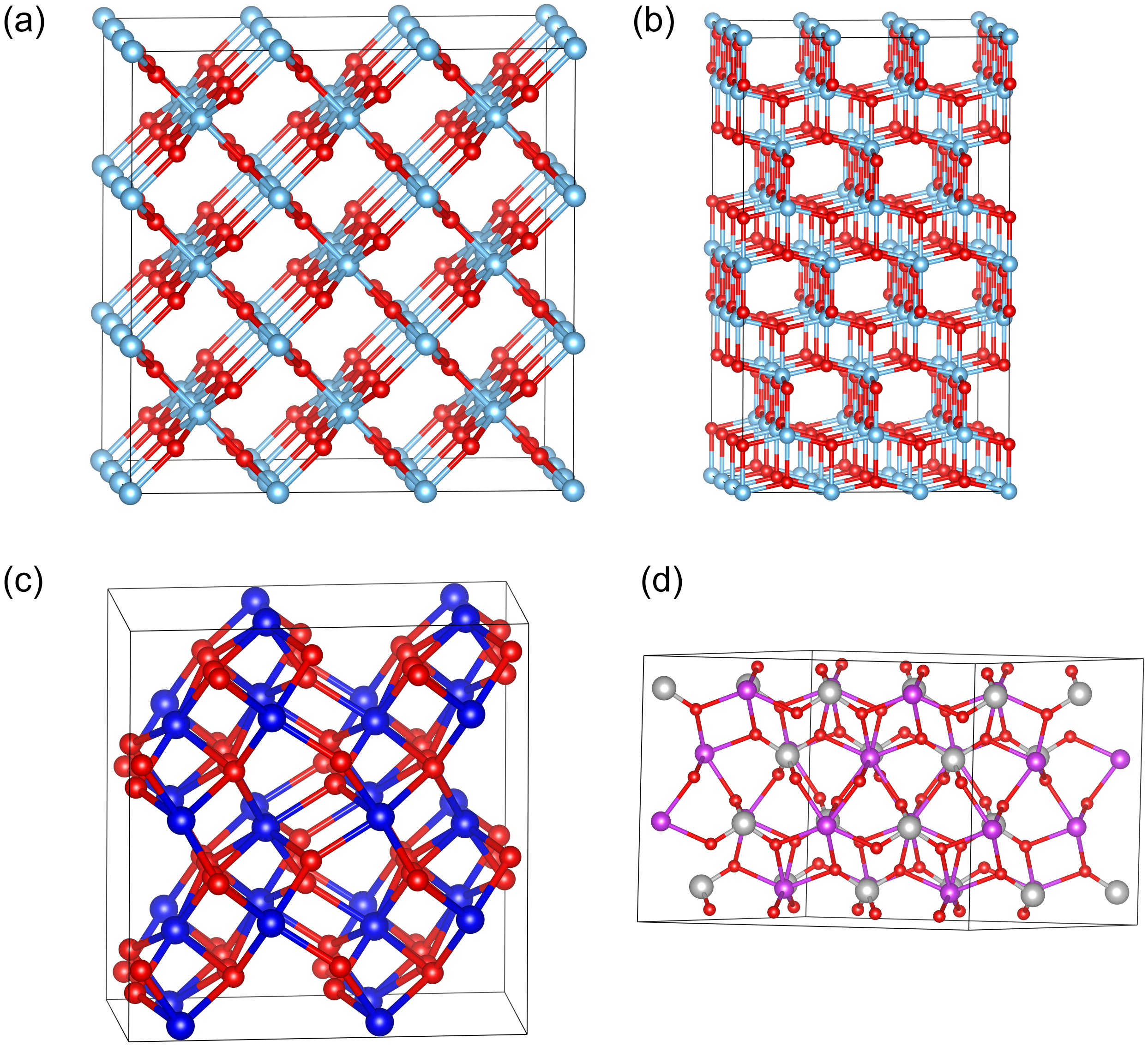

Figure 3: Supercells of (a) TiO_2 rutile, (b) TiO_2 anatase, (c) m-HfO_2 and (d) m-$BiVO_4$. Light blue spheres are Ti, red spheres are O, dark blue spheres are Hf, grey spheres are V and purple spheres are Bi.

was found to be 35.1 $Å_3$ and the optimized lattice parameters were a = 5.14 Å, b = 5.20 Å, c = 5.33 Å, and β = 99.67, in good agreement with experimental[63,64] and theoretical work.[45,65,66] We modelled a supercell of (2x2x2) for m-HfO_2 (Figure 3c), which contained 96 atoms with a size of 10.28 Å x 10.39 Å x 10.66 Å. Reciprocal space was sampled with k-point meshes of 2x2x2.

For monoclinic $BiVO_4$, a kpoint mesh of 8x8x8 was used to optimize the lattice parameters. The equilibrium volume of m-HfO2 was obtained by fitting the DFT energies and volume data with the Murnaghan[62] equation of state. The equilibrium volume was found to be 75.2 $Å^3$ and the optimized lattice parameters were a = 7.33 Å, b = 11.79 Å, c = 5.19 Å, and β = 135.02°, in good agreement with other PBE result.[58,67] We modelled a (2x1x2) supercell for m-$BiVO_4$ (Figure 3d), which contains 96 atoms with a box size of 14.65 Å x 11.79 Å x 10.37. Reciprocal space was sampled with k-point meshes of 2x2x2.

The DFT+U[26] method was used to treat the strong on-site Coulomb interaction of localized electrons. We applied the +U correction on the d orbitals of Ti (TiO_2 anatase and rutile), Hf (m-HfO_2), and V (m-$BiVO_4$). The $U_{effective}$ value we used was in the range of 1 - 10 eV in order to understand how electron localization changes with the $U_{effective}$ value.

For hybrid functional calculations, we used screened hybrid functional proposed by Heyd, Scuseria, and Ernzerhof (HSE06),[68,69] where correlation is described in GGA (PBE) and the exchange is a mixture of 25% exact (HF) exchange and 75% PBE exchange. Because HSE06 calculation is one to two magnitude more expensive that PBE calculation, we use a k-point mesh of 1x1x1 for all our hybrid calculation. Using converged geometries and wavefunction from PBE+U calculations for both cases when polaron is formed and no polaron is formed, we let the system to relax and see whether or not a polaron is formed when we use HSE06.

Traditionally, VASP is run on central processing unit (CPU). In order to reduce the calculation time, effort has been made to increase computer power by parallelization through the usage of multi-core chips, multi-chip nodes, and multi-node computer systems.[70] Recently, VASP has been ported to general purpose graphical processing units (GPU),[70–73] which involves massively parallel processing at low-cost computer systems. This GPU version of VASP allows the simulation of larger and more complex system by reducing the computational cost. In our study, the GPU version of VASP was tested and compared with the standard CPU version of VASP to find the best settings. We chose single metal adsorption on TiO_2 anatase (101) as the study benchmark, based on our previous publication[74] since these CPU results were already available. Figure 4 shows that the GPU settings with high precision (PREC = HIGH) and LREAL = AUTO give best agreement with the CPU calculations, resulting in energy differences of less than 0.02 eV for the tested systems. Therefore, these two settings were used throughout our results.

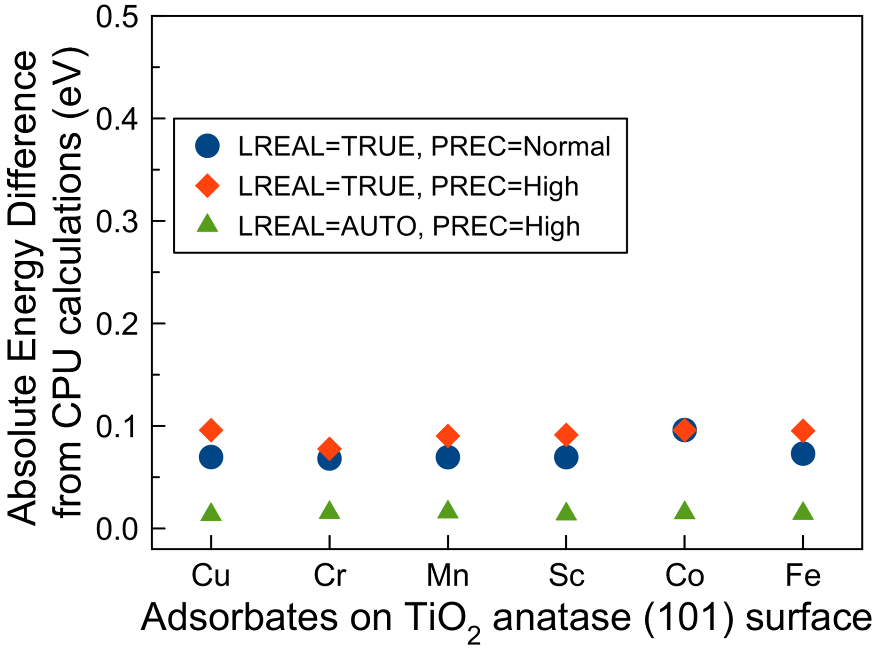

Figure 4: Energy difference for metal adsorption on TiO_2 between the VASP GPU version and CPU version using different settings. The energy of the CPU VASP calculations was taken as the reference energy.

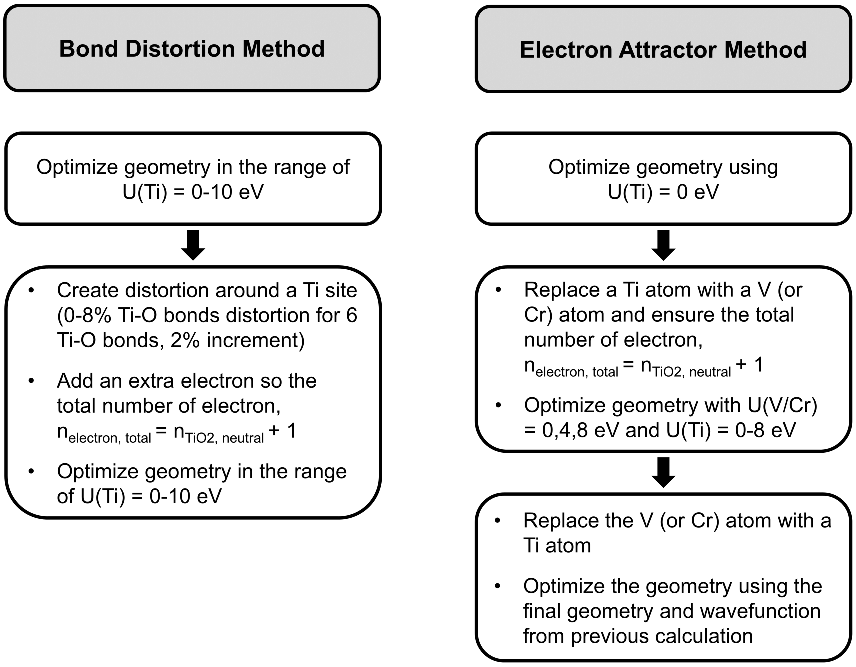

Figure 5: Two methods used to obtain polaron: Bond Distortion Method and Electron Attractor Method

3.2.2 Methods for Modeling Polarons

To model polaron, we added one extra electron to each cell, which was then compensated by a uniform background charge. DFT, DFT+U and Hybrid DFT prefer the delocalized unless certain initial guesses (in terms of geometry and charge density) are given to guide the calculations.[75,76] We explored two methods to model polaron formation, the bond distortion method and electron attractor method (Figure 5). In the bond distortion method the bonds around the preferred polaron site are elongated, while in the electron attractor approach a nucleus with larger positive charge is used to attract electrons to that atomic site. Both methods have been used before.[19,24,25,75,76]

To better assess the stability between a polaron solution and a delocalized solution, we calculated polaron formation energy (E_{pol}), which is the difference between the energy of the polaron solution and the energy of the delocalized solution.

3.2.3 Bond Distortion Method

In this approach a designated atomic position (e.g. Ti in TiO_2) has bonds elongated around that site to mimic the polaronic structure. Electron polarons typically have elongated bonds.[19,22,24] This initial structure is then optimized using DFT and DFT+U. Figure 6 shows examples of TiO_2, where the six Ti-O bonds around a Ti site were elongated by keeping the Ti atom fixed and move the O away from the Ti. The Ti-O bonds were elongated by various degrees,between 0 and 8% for TiO_2. Similarly, for HfO_2, we stretched the seven Hf-O bonds surrounding the Hf site, respectively, by 0%, 2%, 4%, 6% and 8%, and let the system relax. For m-$BiVO_4$, we elongated the four V-O bonds surrounding the V site similarly by 0%, 2%, 4%, 6% and 8%.

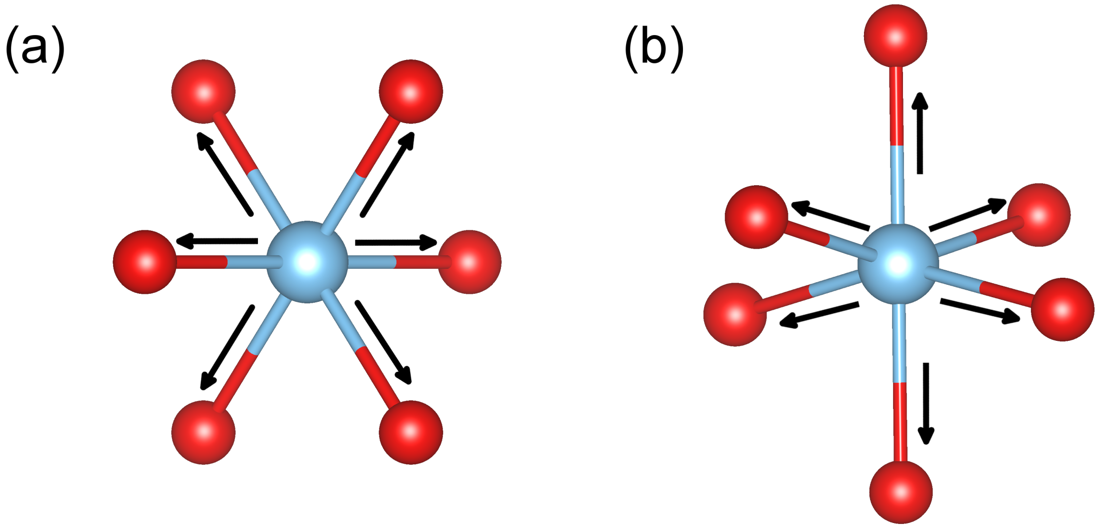

Figure 6: The bond distortion method illustrated for (a) rutile and (b) anatase. Bonds are stretched in the initial geometry in order to create a polaronic-like structure. Optimization of this distorted structure could lead to polaron formation. Blue spheres represent Ti atoms, and red spheres represent O atoms.

3.2.4 Electron Attractor Method

In the electron attractor method. a substituted atom with a more positive nucleus is used to attract an electron to a specific site (e.g. V or Cr in place of Ti). The system with the replaced atom is fully relaxed which may form a polaron structure at the substituted atomic site. The wavefunction and geometry from this calculation are then used for an optimization without the substituted atom. An example for TiO_2 is shown in Figure 7. The total number of electrons of the system with and without the substituted atom are kept the same such that the system without the substituted atom has one extra electron. For m-HfO_2 and m-$BiVO_4$, Ta and Cr were chosen as the substituted atoms, respectively.

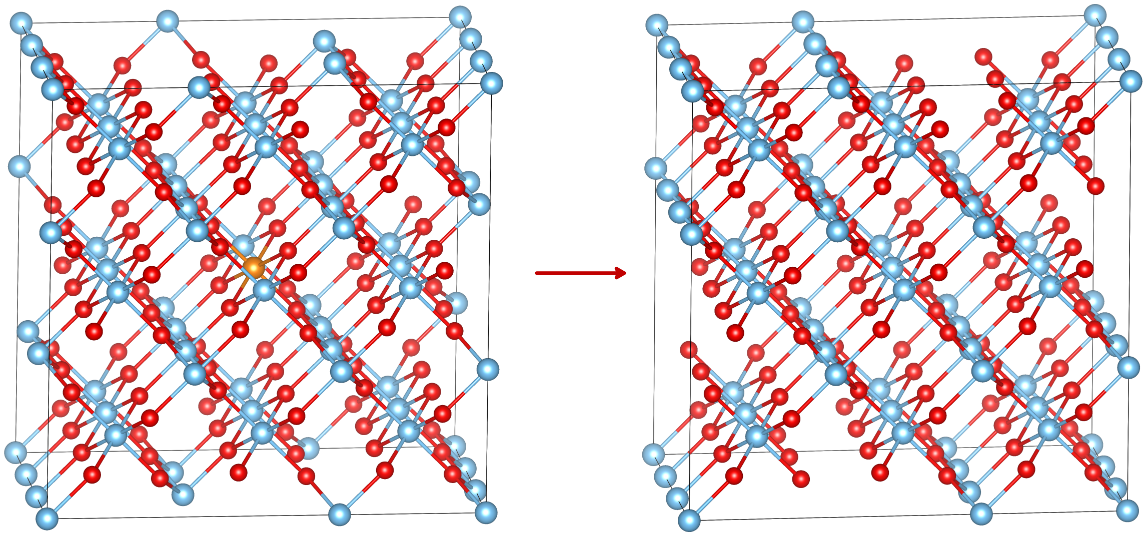

Figure 7: The electron attractor method illustrated for TiO_2 rutile. (a) A supercell with V substituted at a Ti site is optimized, and the converged wavefunction and geometry are then used for a calculation with a (b) supercell only having Ti atoms.

4 Results and Discussion

4.1 Polaron formation in TiO_2

4.1.1 Typical Polarons in TiO_2

In this section, we discuss the typical features of polarons in TiO_2. We verified that a polaron formed using several methods. We visually inspected the spin density to identify the site(s) on which an unpaired electron is localized. Figure 8 shows a spin density plot around the polaronic Ti site for rutile and anatase. Ti sites with no polarons had no spin density.

Quantitatively, we checked if there were lattice distortions surrounding the polaron site compared to the neutral TiO_2 bulk. In Figure 8, the Ti-O bonds surrounding the Ti polaron site are elongated similar to previous literature results.[19–21,77] We also performed Bader charge analysis[78–81] on the charge density and spin density of the system, and compared the Bader charge and Bader spin density with the delocalized solution. For both anatase and rutile, the Bader charge at a Ti polaronic site was about 2.0-2.1, and the charge at a non-polaronic site was in the range of 2.3-2.5. Non-polaronic Ti sites always give values of 0e for the Bader spin density, while polaronic sites give spin density of 0.70e - 0.95e for both rutile and anatase, in agreement with results from Chrtien et al.[25] for the TiO_2 rutile (110) surface.

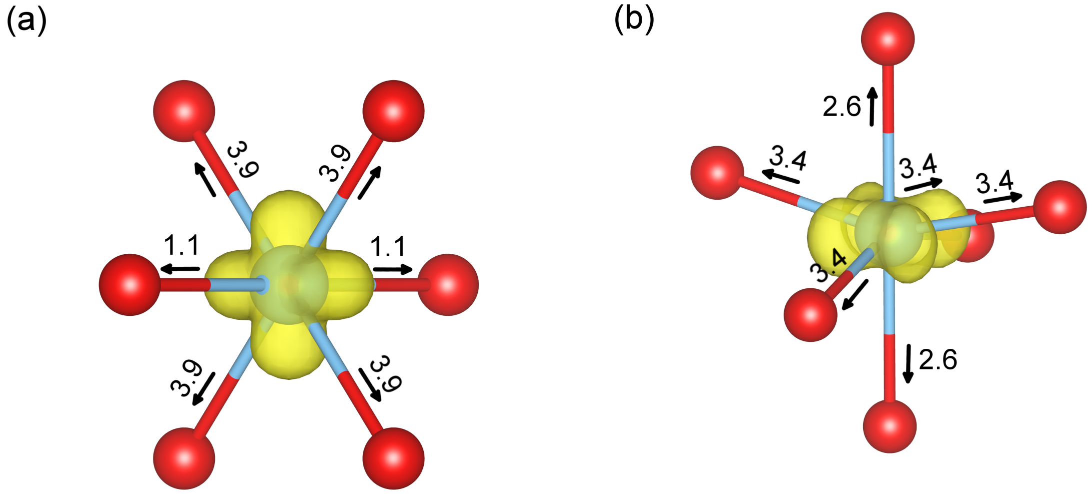

Figure 8: Example polarons formed in (a) rutile and (b) anatase. Shown are spin density plots around the polaronic Ti site. The numbers show the % that the Ti-O bonds increased upon polaron formation. U values of 3 eV (rutile) and 4 eV (anatase) were used for these structures.

4.1.2 Bond Distortion Method

The bond distortion method attempts to create an initial structure that mimics the polaron so that optimization to the polaronic state becomes easier. For TiO_2, we distorted the bonds around a chosen Ti atom by extending the Ti-O bonds (through moving the O atoms and keeping the Ti atom fixed) by 0, 2, 4, 6, and 8% relative to the non-distorted bulk structure. We also used U values between 1 and 10 eV on the d-orbitals of the Ti atoms. These combinations of bond distortions percentages and U values allowed us to assess which parameters could be ideal for modeling polarons.

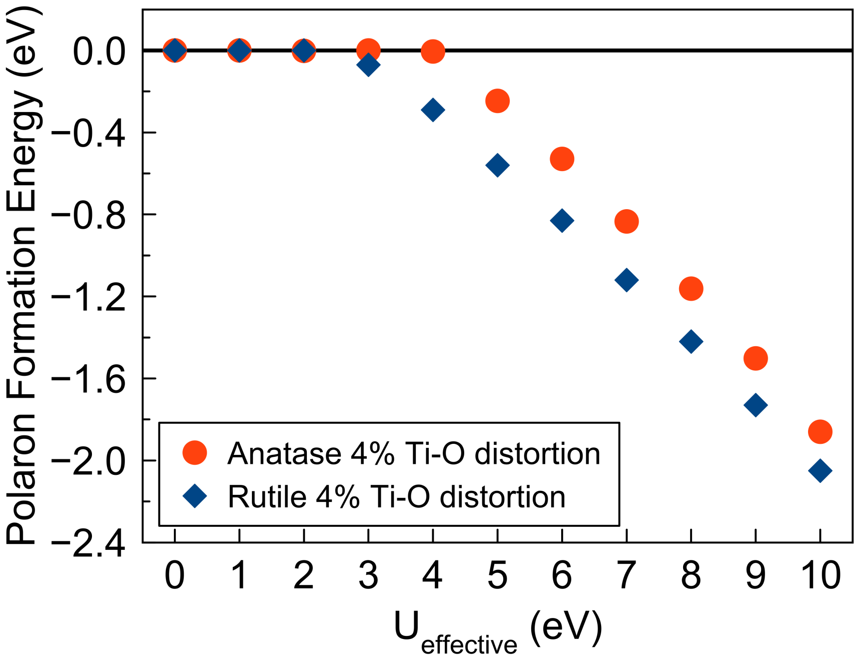

Figure 9: Polaron formation energies in (a) rutile and (b) anatase using different U values. Shown are results for a 4% initial Ti-O bond lengthening. Polarons only started to form when $U \geq 3$ eV in rutile and $U \geq 4$ eV in anatase. At these U values, 4, 6 and 8 % distortion gave similar polaron results. The 2% distortion results formed polarons only for $U \geq 4$ eV for rutile and $U \geq 5$ for anatase. Polarons do not form when no initial distortions were present, regardless of the U value. The complete polaron formation energies are shown in the Appendix, Table A1 and A2.

We found that without any initial distortion (0% Ti-O distortion), electrons always delocalized throughout the system, no matter what U value was employed. Polaron formation only occurred when an initial distortion was introduced to the bulk TiO_2. We also found that the 6% and 8% Ti-O bond distortions always converged to the same solutions as the 4% distortion results. A 2% distortion required larger U values ($U \geq 4$ eV for rutile and $U \geq 5$ eV for anatase) than a 4% distortion ($U \geq 3$ eV for rutile and $U \geq 4$ eV for anatase) to form a polaron, but converged to the same solution as the 4% distortion results when the polaron formed. A full listing of all formation energies at each U value is given in the Appendix, Table A1 and A2.

Polaron formation energies (E_{pol}) with different $U_{effective}$ values for rutile and anatase are shown in Figure 9 for calculations with initial 4% Ti-O bond lengthening. As mentioned earlier, because 4, 6 and 8% distortion always give similar results and 2% distortion only gives polaron solution at larger U values than 4% distortion, we only show the results using 4% Ti-O bond distortion in Figure 9. We found that polarons formed when $U \geq 3$ eV for rutile and $U \geq 4$ eV for anatase, in good agreement with previous theoretical work.[20,25]

We found that as the U value increases, the polaron formation energy increased, in agreement with previous GGA+U calculation on polaron formation in TiO_2.[19,20] We also saw that polaron formation energies for rutile were lower than for anatase by ~ 0.3 eV, in agreement with previous theoretical results[20,21] showing a polaron is more likely to form in rutile than in anatase.

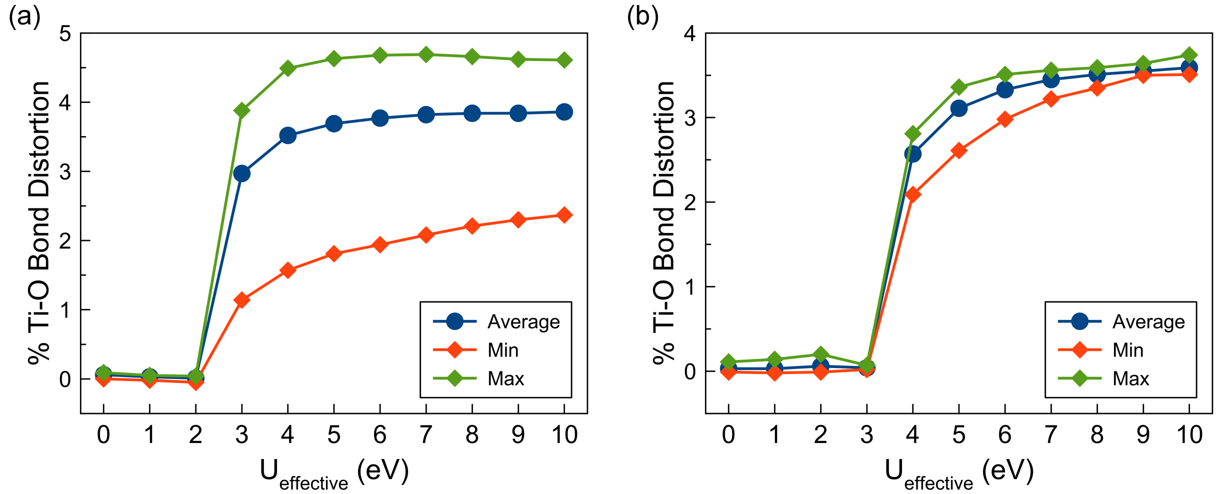

Figure 10: Final average, minimum, and maximum Ti-O bond elongations at different U values starting from an initial 4% distortion. Results are for (a) rutile and (b) anatase. Polaron is formed when $U \geq 3eV$ for rutile and $U \geq 4$ eV for anatase, as evidenced by the Ti-O elongations.

Figure 10 shows the average, minimum and maximum Ti-O bond elongations after convergence at different U values. For a given delocalized solution (U less than 3 eV for rutile and U less than 4 eV for anatase), the geometry was similar to the original bulk geometry. On the other hand, when a polaron formed, the average, minimum and maximum final bond elongations increased and eventually reached common values. For rutile, the common values for the average, minimum and maximum %Ti-O bond distortion are 3.9%, 2.4% and 4.6 %. These values for anatase are 3.6%, 3.5% and 3.7%, respectively. As a result, 4% initial Ti-O bond distortion for rutile and anatase gave initial guesses very close to the polaron structure. As we will discuss later on, 4% distortion also resulted in the fastest convergence.

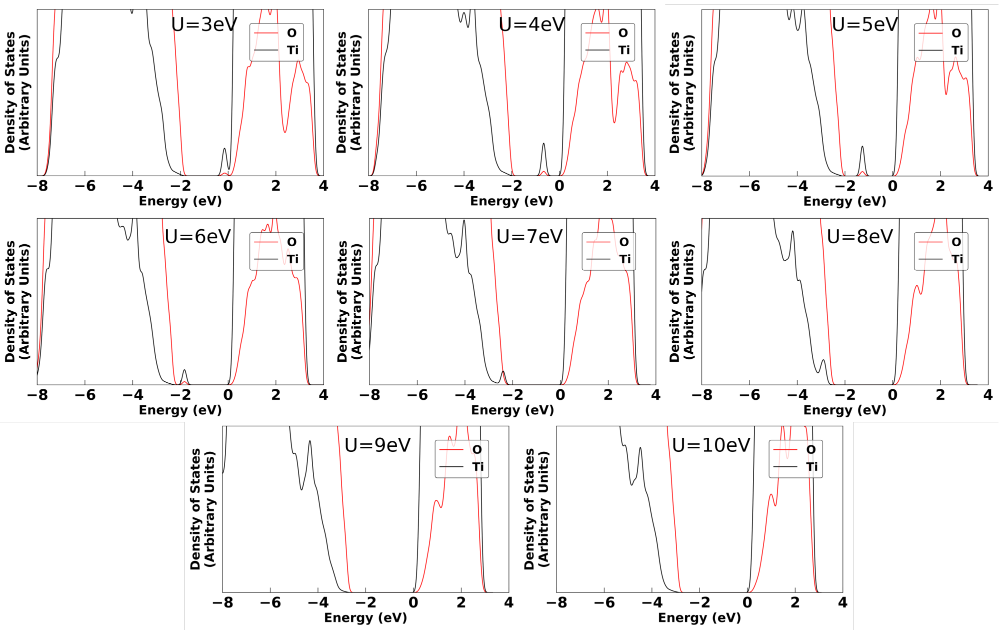

Figure 11: Projected density of states for TiO_2 rutile using different U values where a polaron formed. The zero energy is chosen as the conduction band minimum (CBM). The polaron exists as a small gap state predominantly on Ti atoms. At U values of 9 and 10 eV, the polaron was completely within the valence band.

In Figure 11, we show the calculated density of states for TiO_2 rutile at different U values where a polaron formed. Similar plots for anatase is shown in the Appendix, Figure 1. At low U values (U = 3 eV), the polaronic state is located near the conduction band minimum (CBM). As the U values increased, the polaronic state shifted toward the valence band maximum (VBM) before completely merging into the VBM (U = 8eV). Experimentally, the polaron state below conduction band minimum is about 0.7 eV for rutile[20,77] and 1 eV for anatase.[20] The polaron location with respect to the conduction band will be discuss further in Section 4.1.4.

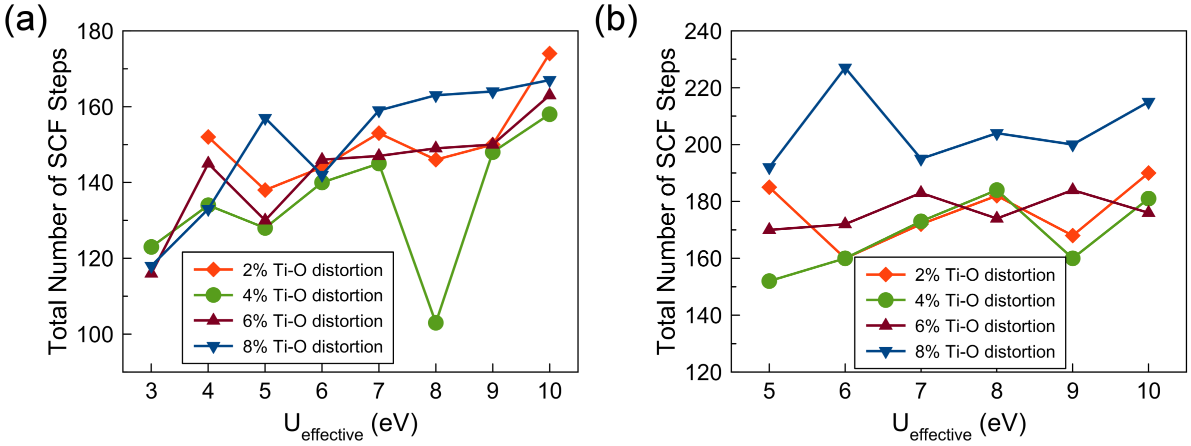

Figure 12: Total number of self consistent field (SCF) steps needed for complete geometry optimization for the cases when a polaron formed in (a) rutile and (b) anatase.

We examined how long different initial distortion would take to converge to a final polaron structure. In general, 4% bond distortion gave the smallest number of geometry steps for both rutile and anatase. Figure 12 shows the total number of self-consistent field (SCF) steps needed to converge to a polaron solution starting with different %Ti-O bond distortion levels and at different U values. The number of SCF steps was summed up from all the geometry steps. The number of geometry steps for each case are given in Figure ??. For rutile the number of SCF steps generally increased with increasing U values, but this relationship was not as strong for anatase. An initial 4% Ti-O bond distortion generally led to the smallest number of SCF steps to reach convergence. The 4% distortion case better mimicked the final polaron solution, which could explain why it generally required the fewest number of steps to converge. In general, however, there was not a strong relationship between number of SCF steps and initial % distortion.

To conclude, we showed that for both rutile and anatase, polaron formation requires initial distortion around the Ti polaron site and at least moderate U values applied to d orbitals on Ti atoms. When a polaron was formed, different initial distortions converged to the same polaron solution. We also showed that an initial 4% bond distortion gave the best results in both forming a polaron and in the calculation speed. The 4% distortion is closest to the final solution, which explains why this % distortion worked so well.

4.1.3 Electron Attractor Method

The electron attractor method attempts to create a polaronic state by localizing an unpaired electron on a designated site using atoms (V or Cr) that have more positive nucleus than Ti, or by substituting atoms that attract electrons more than other lattice atoms. For the substituted atoms (V or Cr), we employed U values of 0, 4 and 8 eV, and for the Ti atoms, we employed U values between 1 and 8 eV. These combinations of different atom substitutions (V and Cr), U values on the substituted atoms, and U values on Ti allowed us to assess which parameters could be ideal for modeling polarons.

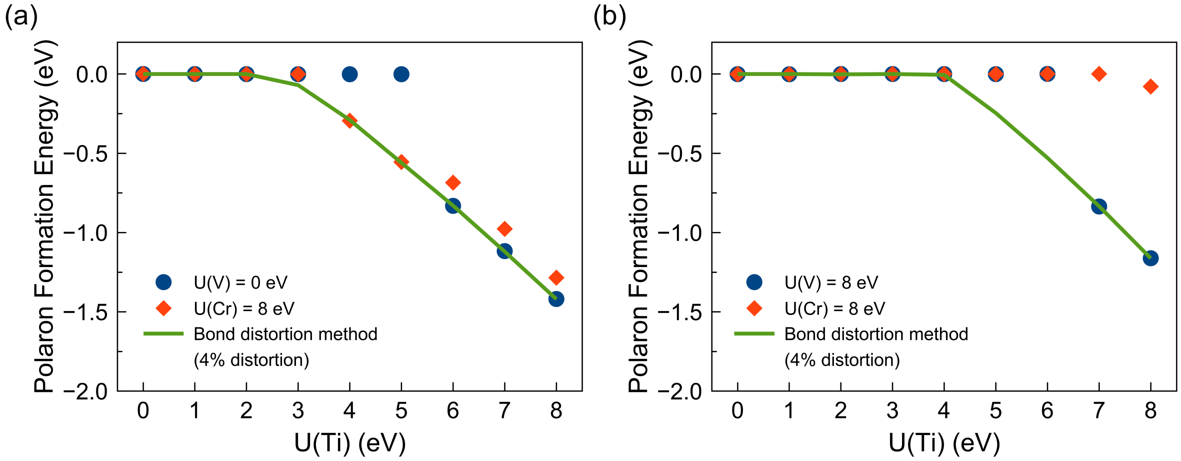

Figure 13: Polaron formation energies in (a) TiO_2 rutile and (b) TiO_2 anatase using the electron attractor method. U(Ti), U(V) and U(Cr) represent the U values employed on Ti, V and Cr, respectively. For each substituted atom (V or Cr), data is shown for the results that give the closest results compared to the bond distortion method (4% distortion). A complete listing of the polaron formation energies using the electron attractor method is shown in the Appendix, Table A3 and A4.

Figure 13 shows the polaron formation energies for rutile and anatase using V and Cr substitutions. For each substituted atom, we chose to only show the results at certain U values applied on V/Cr (U(V)/U(Cr)) that gave the closest results to the bond distortion method in terms of polaron formation energy The U values employed on Ti atoms (U(Ti)) were varied for different calculations.

For rutile, polarons formed when the combination of U(V) = 0 eV and $U(Ti) \geq 6$ eV or the combination of U(Cr) = 8 eV and $U(Ti) \geq 4$ eV were used (Figure 13a). Using V-substitution, when a polaron was formed, the polaron solution was found to be similar to that found by bond distortion method, in terms of the polaron formation energy, the lattice distortion surrounding the polaron site and the Bader charge. Using Cr-substitution, when U(Ti) = 4 and 5 eV, similar polaron structures to bond distortion method were found; however, when U(Ti) = 6-8 eV, less stable polaron structures were obtained. For anatase, we found that polarons formed when U(V) = 8 eV and $U(Ti) \geq 7eV$. No polarons formed using Cr substitution with anatase (Figure 13b). When a polaron formed using V-substitution, the polaron structure was similar to that obtained by the bond distortion method. It should be noted that using the bond distortion method, a polaron formed when $U(Ti) \geq 3eV$ for rutile and $U(Ti) \geq 4eV$ for anatase. Using the electron attractor method, polarons formed when $U \geq 4eV$ for rutile using Cr-substitution and $U \geq 7eV$ for anatase using V-substitution. Therefore, we conclude that the electron attractor method did not predict polaron formation at low U(Ti) values, while the bond distortion method did.

To explain why the electron attractor method did not form polarons at small U(Ti) values, and why it also gave several less stable polaron structures than the bond distortion method, we examined at the geometry of the converged solution after replacing Ti with V or Cr (but before the substituted atom was removed and replaced by Ti). Figure 14 shows the V-O or Cr-O bond length distortions compared to neutral TiO_2. For rutile (Figure 14a), the average V-O bonds were shortened after relaxation, giving an unfavorable starting geometry for the final polaron calculations; polarons in TiO_2 elongate Ti-O bonds. On the other hand, Cr-O bonds were elongated, giving a favorable starting geometry for final polaron calculations. The bond lengths also explain why Cr-substitution results agree more with the bond distortion method, than the V-substitution results (Figure 13a). For anatase (Figure 14b), both the

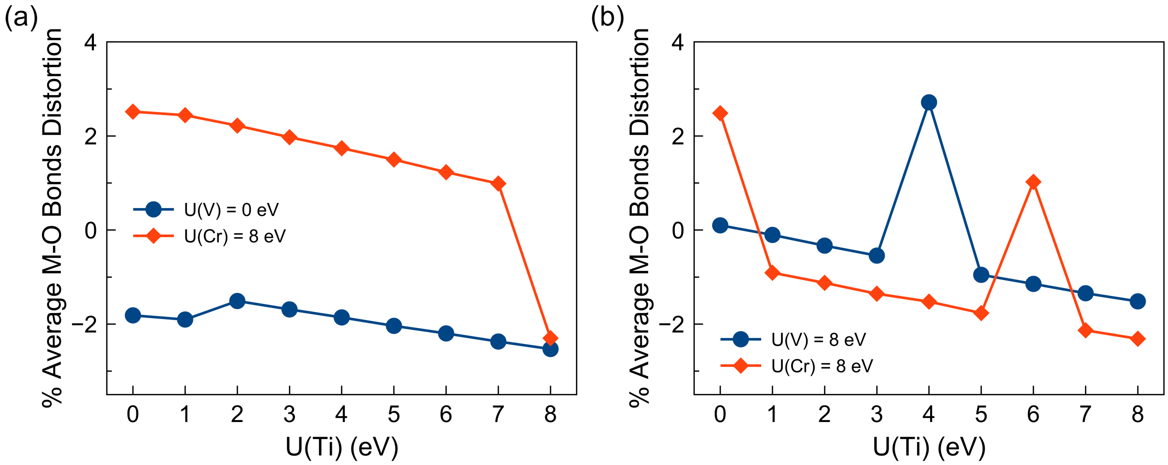

Figure 14: Average M-O bond length distortions (compared to bulk TiO_2) for optimized structures with one Ti atom substituted by V or Cr. (a) TiO_2 rutile and (b) TiO_2 anatase. M represents V or Cr.

average V-O and Cr-O bonds were shortened after relaxation, except for the combinations of U(V) = 8 eV and U(Ti) = 0 and 4 eV, and U(Cr) = 8 eV and U(Ti) = 0 and 6 eV. Similar to rutile, these shortened V-O and Cr-O bonds created an unfavorable starting geometry for final polaron calculations since polarons elongate Ti-O bonds.

We originally hypothesized that using substituted atoms with more positive nuclei would attract electrons, which would create better geometries and wavefunctions for polaron formation calculations. We calculated the Bader spin charge of the substituted atoms, V or Cr, as shown in Figure 15. These results are for structures before the V/Cr was removed and replaced by Ti atoms. For rutile (Figure 15a), results from the bond distortion method showed that upon polaron formation, the Bader spin charge of the Ti polaron site was about 0.9e-. V-replacement gave good agreement in terms of the spin charge, while Cr-replacement overestimates the spin charge of the polaron site. Incorrect initial wavefunctions might be the reason that using Cr-replacement led to less stable polaron structures in rutile at U(Ti) = 6-8 eV (Figure 13a). Similarly, incorrect initial wavefunctions might be the reason for no polaron formation when Cr substitution was used in anatase.

Figure 16 shows the total number of SCF steps compared between the electron attrac-

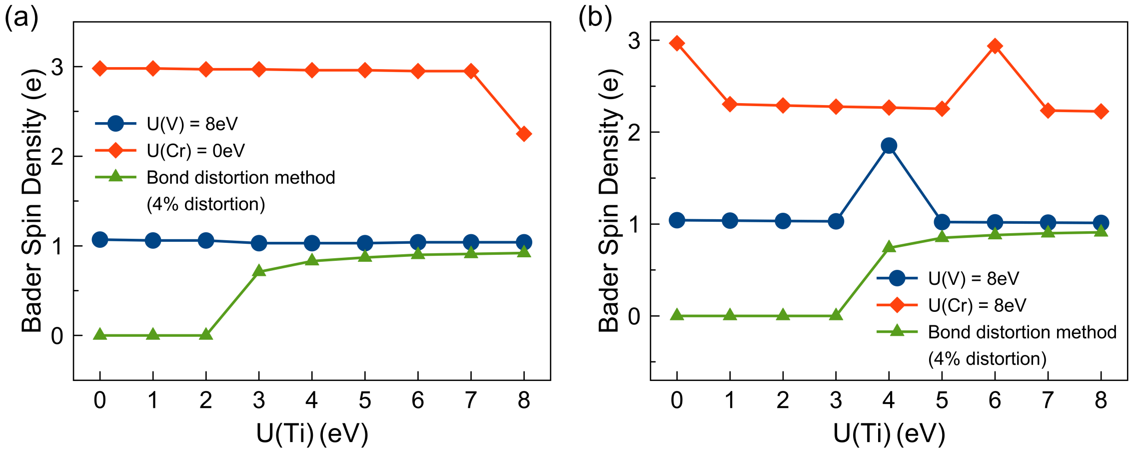

Figure 15: Bader spin charges for optimized structures with one Ti atom substituted by V or Cr. Results are shown for the substituted atom in (a) TiO_2 rutile and (b) TiO_2 anatase. For comparison spin densities of polaronic Ti atoms using the bond distortion method are shown.

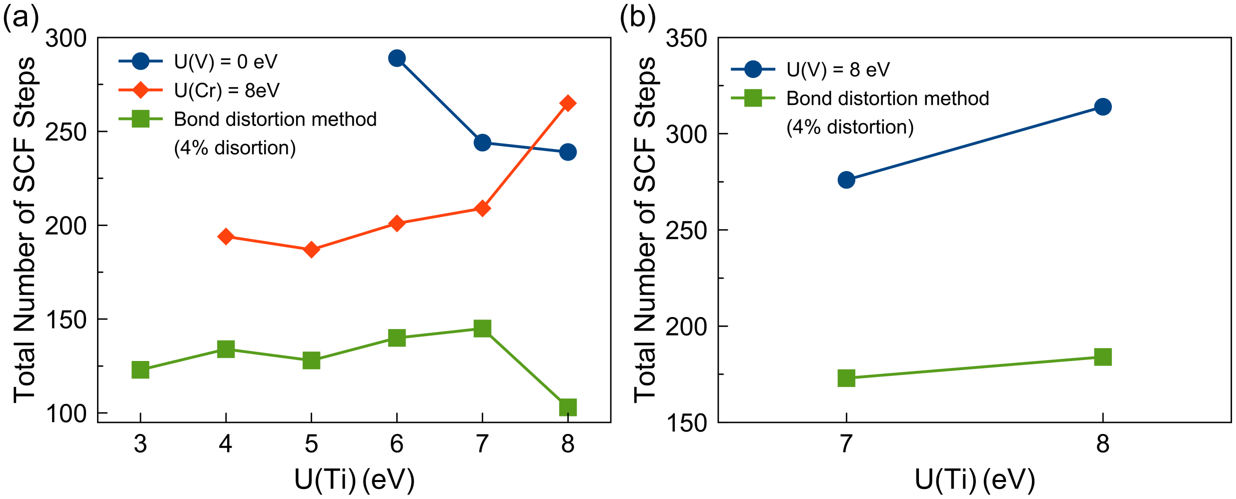

Figure 16: The total number of SCF steps for calculations in which polarons formed using the electron attractor method for (a) rutile and (b) anatase.

tor method and bond distortion method (4% distortion) for calculations in which polarons formed. The bond distortion method required e a smaller number of SCF steps than the electron attractor method for both rutile and anatase. The bond distortion method started with a geometry closer to the actual polaronic state than the electron attractor method, which is why fewer steps were required. For rutile, Cr-replacement generally required smaller number of SCF steps than V-replacement because the geometry generated using Cr-replacement was closer to the correct polaron solution (Figure 14a). In general, it appeared that the electron attractor method might give dubious results and may not be an effect way to model polarons.

4.1.4 Polarons and Hybrid Functionals with TiO_2

Hybrid functionals, HSE06[68] in particular, have been shown to better describe the electronic structure of TiO_2[82] than pure DFT or DFT+U calculations. Therefore, we employed the HSE06 functional to study polaron formation in TiO_2. We compared the HSE06 results with the DFT and DFT+U results. It has been known that the HSE06 functional is much more computational expensive than DFT+U calculations. To reduce the computational cost and speed up convergence of the HSE06 calculations, we used previously converged geometries and wavefunctions from GGA+U calculations as starting points for the HSE06 calculations. We used the converged solutions from U = 6 eV for both rutile and anatase. The converged polaron geometry and wavefunction was obtained from 4% distortion calculations and the converged delocalized solution was obtained from 0% distortion for both rutile and anatase. We chose to start from both delocalized and localized GGA+U solutions to determine the effect on polaron formation using the HSE06 functional. It would also be interesting to use the converged solutions from other U values, but because of time constraint, we were not able to do so.

For rutile, we found that a polaron was formed only when we started with a polaron solution as the initial guess. Delocalized HSE06 solutions always occured when we started with GGA+U delocalized geometries/wavefunctions. The polaron formation energy was -

0.59 eV using HSE06, which is equivalent to results obtained from GGA+U with $U \sim 5$ eV. The Bader charge on the polaron Ti atom was 2.1 e-, and the Bader spin density value was 0.72 e-. For TiO_2 anatase, no polaron solution was obtained when starting from either localized or delocalized GGA+U geometries/wavefunctions. This result for anatase agrees with previous results from Spreafico et al.,[21] who showed that using HSE06 (25% HF exchange) and a small supercell, the delocalized solution is more favorable than the polaronic solution in anatase. Spreafico et al. also noted that when using a bigger supercell and higher %HF exchange, polaronic solution were obtained in anatase. As a result, we suspect that simulation of a larger anatase supercell might lead to a polaron.

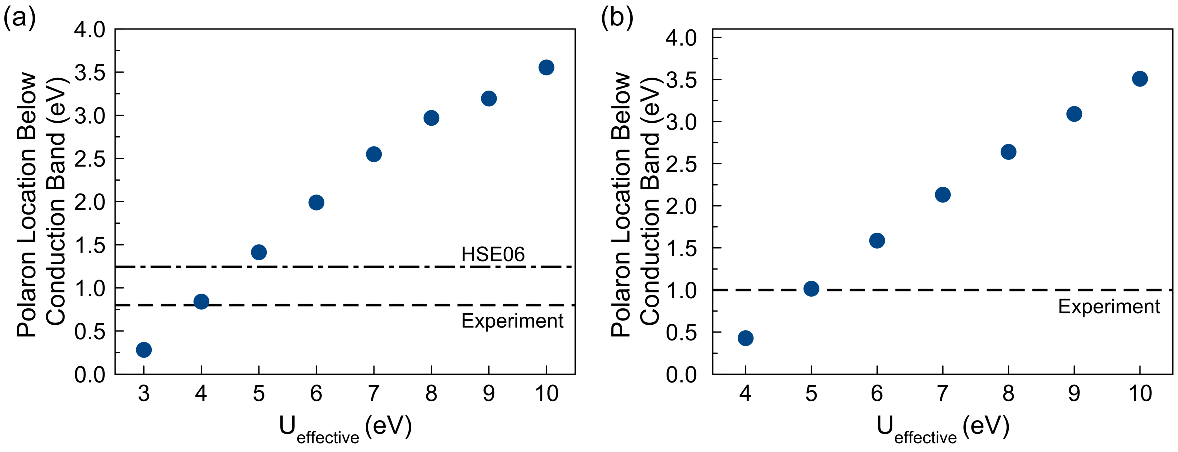

Figure 17: Energy location of polaron states obtained from GGA+U, HSE06, and experiments for (a) rutile and (b) anatase. No polaron formed using HSE06 for anatase. Experimental results are from Setvin et al.[20]

To validate our simulation results, we compared the calculated polaron energy locations (with respect to the conduction band) using GGA+U and HSE06 to experiment results (Figure 17). Experimentally, the small polaron state is about 0.7 eV below the conduction band minimum (CBM) in rutile[20,77] and about 1 eV below the conduction band minimum for anatase.[20] For rutile, Figure 17a shows that HSE06 overestimated the polaron location by about 0.5 eV. The polaron location in the GGA+U calculations, on the other hand, depended on the U value employed. To obtain a polaron state similar to the experimental polaron state, a U value of about 4 eV should be used for rutile. For anatase, no polaron was formed using HSE06. For the GGA+U calculations, the polaron location also depended on the U value being applied (Figure 17b). To obtain a polaron state similar to the experimental polaron state, a U value of about 4 eV should be used for anatase. It also should be noted the Setvin et al.[20] experimentally found two different polaron states for anatase, with a small polaron (mentioned earlier) located about 1 eV below the CBM and a large polaron about 0.04 eV below the CBM. The type of polaron, according to Setvin et al., depended on the source of the extra electrons: Oxygen vacancies in TiO_2 resulted in small polaron formation and Nb doping in TiO_2 resulted in large polaron formation. Therefore, as mentioned earlier, a larger supercell for anatase might be needed to model polarons, since a small supercell may not accommodate a large polaron.

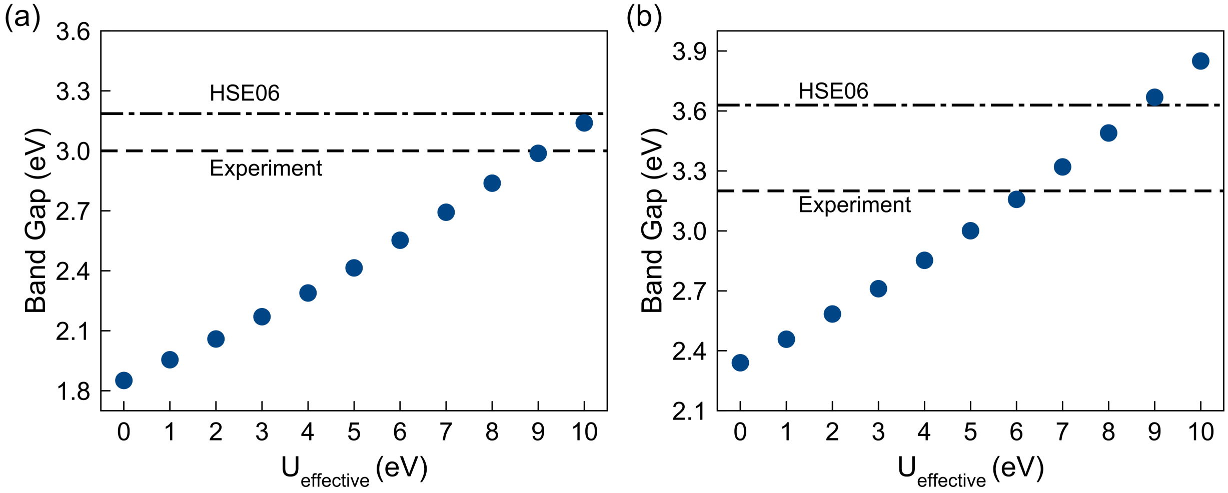

Figure 18: Band gaps obtained from GGA, GGA+U and HSE06 calculations, and experiments for (a) rutile and (b) anatase. Experimental band gaps for rutile and anatase were obtained from Tang et al.[83] and Pascual et al.,[84] respectively.

Another important feature of semiconductors is the band gap. Figure 18 shows the band gap obtained from GGA, GGA+U, HSE06 calculations, and experimental results. Experimentally, the band gap is near 3.0 eV for rutile[83] and 3.2 eV for anatase.[84] Figure 18 shows that GGA calculations severely underestimated the band gap in both rutile and anatase. With GGA+U, by increasing the U values, we obtained the experimental band gap of both rutile and anatase using U = 9 and 6 eV, respectively, similar to previous GGA+U calculations.[19] We found that HSE06 slightly overestimated the band gap of TiO_2 rutile and anatase, giving band gaps of 3.19 eV and 3.63 eV, respectively. These calculated band gaps are in good agreement with other HSE06 calculations,[82] which found the band gaps of rutile and anatase to be 3.37 eV and 3.58 eV.

To summarize, we showed that both GGA+U and HSE06 can be used to model polarons in rutile. HSE06 slightly overestimated the polaron state location below the conduction band. By tuning the U value, GGA+U was able to obtain the experimental polaron location. Similar, by tuning the U value, GGA+U could obtain the polaron location in the band gap for anatase. HSE06 did not form a polaron in anatase, but as explained earlier, increasing the anatase supercell size might facilitate polaron formation. HSE06 was better at describing the band gap for TiO_2 than pure DFT, but the associated computational cost of employing HSE06 was much larger than using DFT+U.

4.2 HfO_2

4.2.1 Typical polaron formation in m-HfO_2

Similar to previous polaron calculations with TiO_2 rutile and anatase, we verified that polarons formed in m-HfO_2. We examined the spin density to see if there was electron localization on certain Hf sites. Figure 19 shows the spin density around the polaronic Hf site(s) for m-HfO_2. Non-polaronic Hf sites will have no spin density. Figure 19a shows that at U = 6 eV, the unpaired electron was localized on three neighboring Hf atoms that shared a mutual O atom. Figure 19b shows that at U = 8 eV, the unpaired electron was completely localized on a single Hf atom. We also performed Bader charge analysis[78–81] on the charge density and spin density of the system. We compared the Bader charge and Bader spin density with the delocalized solutions. The Bader charge of a polaronic Hf atom was 2.3-2.5 e-, while non-polaronic Hf atoms had a charge of 2.7-2.8. The Bader spin density charge of a polaron site was 0.3e - 0.8e and of a non-polaron site was 0 e-. Furthermore, we checked if there were

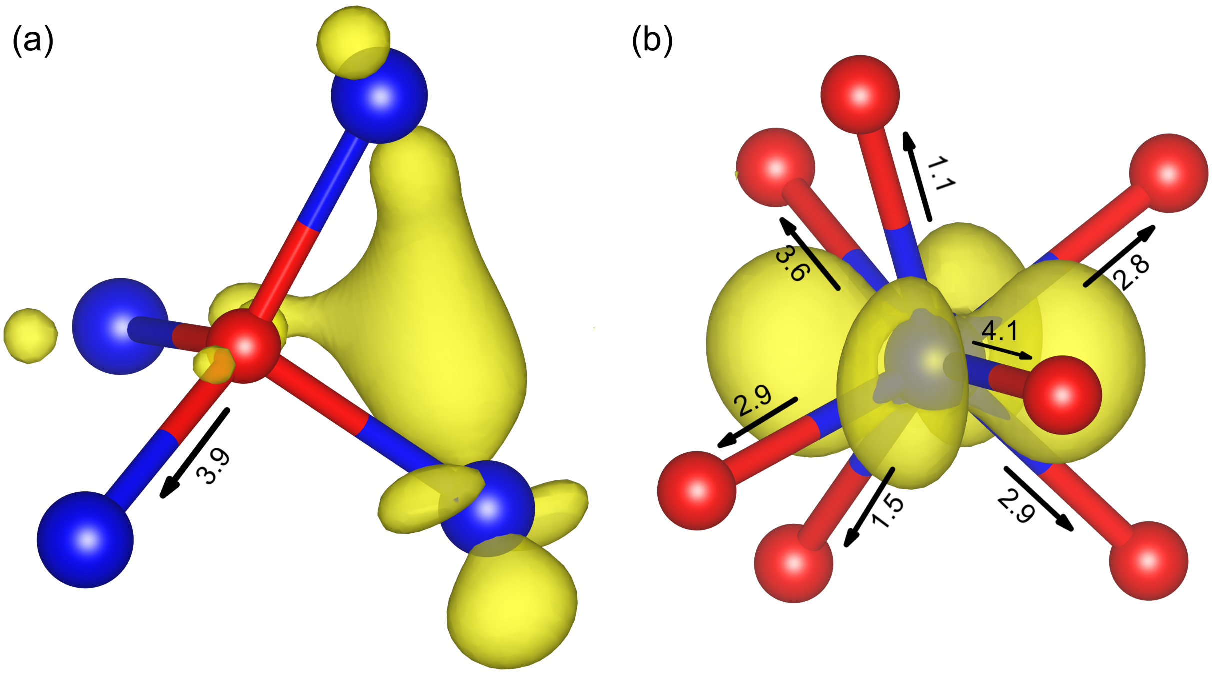

Figure 19: Example polarons formed in m-HfO_2 using 4% initial Hf-O bond distortion with (a) U(Hf) = 6eV and (b) U(Hf) = 8eV. Shown are spin density plots around the polaronic Hf site(s). The numbers show the % that the Hf-O bonds increased upon polaron formation. Blue spheres represent Hf atoms and red spheres represent O atoms.

lattice distortions surrounding the polaron site(s) compared to the neutral m-HfO_2 bulk. In Figure 19a, the three Hf-O bonds of the three Hf polaron sites remained the same, while the fourth Hf-O bond was elongated. In Figure 19b, the seven Hf-O bonds surrounding the Hf polaron site were elongated.

4.2.2 Bond Distortion Method

We found that without and initial distortion of Hf-O bonds, no polaron was formed, regardless of the U value applied. When a polaron was formed, 2, 4, 6 and 8% distortion converged to the same solution. However, different combinations of U value and % distortion dictated whether a polaron formed or not (Appendix, Table A4). For instance, when a U = 7 eV was employed, 2, 4 and 6% initial distortions converged to the same polaron solution, but a 8% distortion relaxed to a delocalized solution. Another example was when U = 10 eV was employed, the 4,6 and 8% distortions converged to the same polaron solution, but the 2%

distortion relaxed to a delocalized solution.

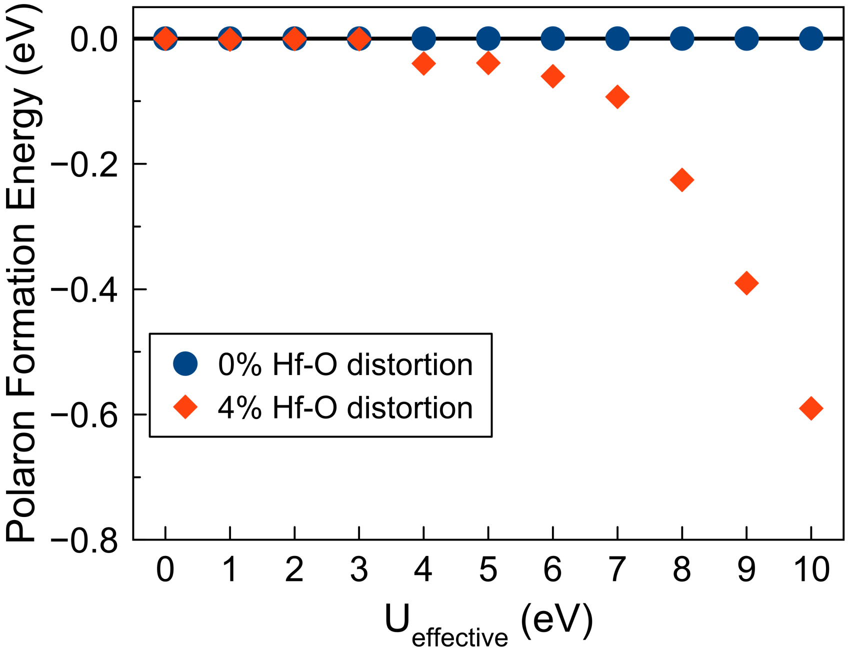

Figure 20: Polaron formation energies in m-HfO_2 compared to the U value on Hf. Results show results for 0% and 4% initial Hf-O bond distortions. No polaron is formed without initial distortion, no matter what U value was employed. Polarons formed when $U \geq 6eV$ using 4% Hf-O bond distortion. For 4% Hf-O distortion, at U = 4 and 5 eV, the distortion converged to a slightly more stable structure, but no polaron was formed. A full listing of polaron formation energy is shown in the Appendix, Table A5.

Figure 20 shows the polaron formation energies at different U values for two different initial Hf-O bond distortion levels (0% and 4% distortion). We found that a polaron formed with $U \geq 6$ eV if a bond distortion was applied to the initial geometry. We note that at lower U values (U = 4 eV and 5 eV), the initial distortion led to a slightly more stable geometry (as indicated in Figure 20, by the energies being negative), but no polaron was actually formed at these U values. As the U values increased, polaron formation became more favorable compared to delocalized solutions, similar to the TiO_2 results.

We found that the choice of U value significantly affected the polaron solution. At U = 6 eV, the unpaired electron was disproportionately distributed on three neighboring Hf

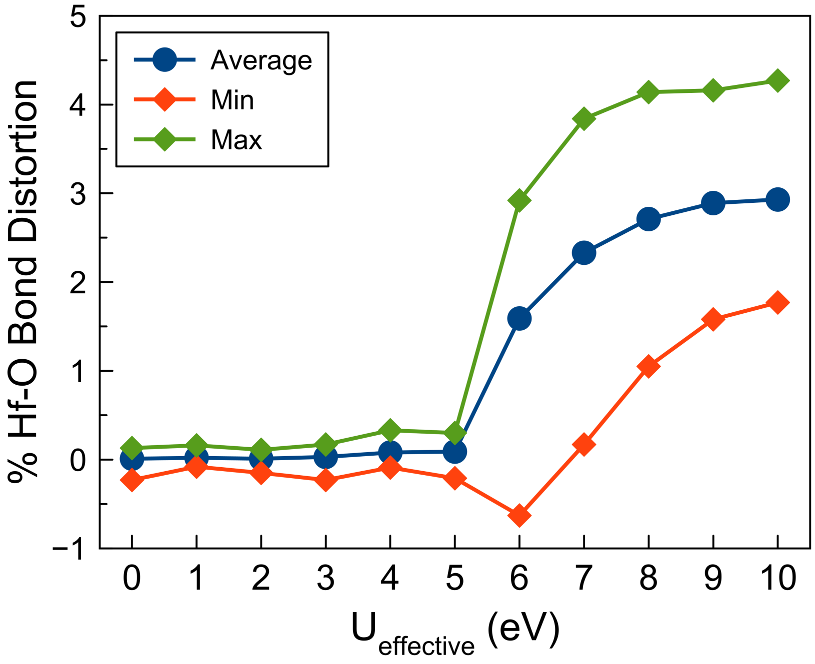

Figure 21: Final average, minimum and maximum Hf-O bond lenght elongations surrounding the Hf polaronic site at different U values using initial 4% Hf-O distortion. For cases in which electron is localized on three Hf atoms (U = 6 and 7 eV), the Hf atom with the highest Bader spin density was chosen as the polaronic site.

ions sharing a four-coordinated O atom (Figure 19a). The Bader spin charges distributed on these three Hf ions were 32%:12%:10%, with the rest of the spin density on other O and Hf ions in the cell.The sharing of the extra electron on 3 neighboring Hf ions was similar to results obtained by Ramo et al.,[24] who used a B3LYP hybrid functional. However, as the U value increased, the unpaired electron became fully localized on a single Hf site, as shown in Figure 19b. Similar to results for TiO_2, as the U value increased, the polaron became bigger as the average, minimum and maximum Hf-O bonds surrounding the Hf polaronic site increased and eventually reached common values of 2.9%, 1.8% and 4.3%, respectively (Figure 21).

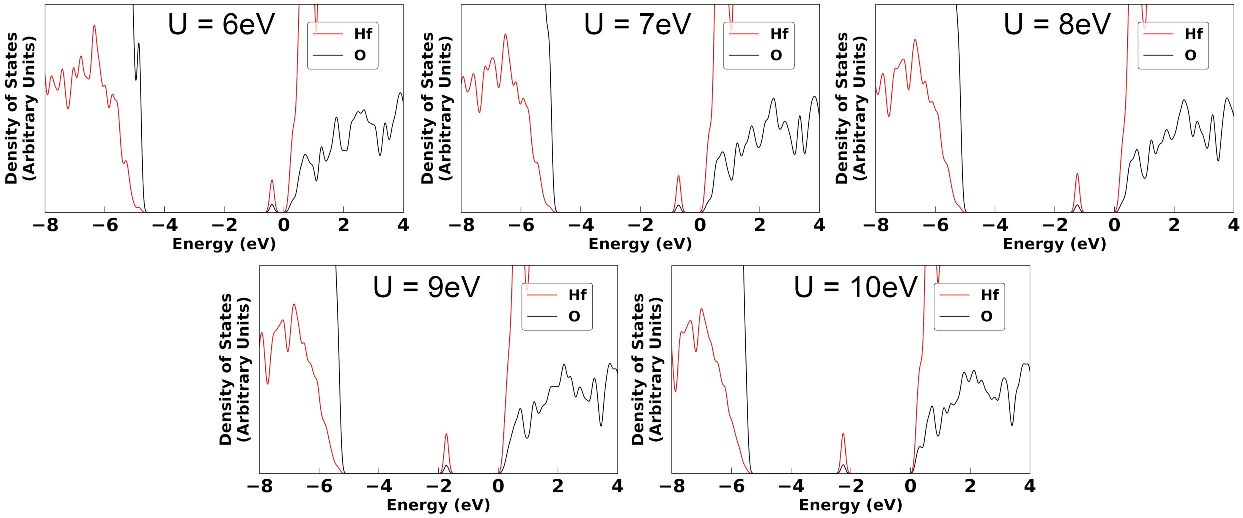

Figure 22: Projected density of states for m-HfO_2. The zero energy was chosen as the conduction band minimum (CBM).

In Figure 22, we show the calculated density of states for m-HfO_2 at different U values where a polaron was formed. When a polaron was first formed (U = 6 eV), the polaronic state was located near the conduction band minimum (CBM). As the U values increased, the polaronic state shifted toward the valence band maximum (VBM). Because polaron was formed in m-HfO_2 at higher U values ($U \geq 6$ eV) than in TiO_2 ($U \geq 3$ eV for rutile and $U \geq 4$ eV for anatase), and the band gap of m-HfO_2 (5.7 eV experimentally[85]) is greater than that of TiO_2, the polaron state did not reach the valence band at U = 10 eV for m-HfO$_2$. If we applied a higher U value on Hf atoms, we would expect similar results to TiO$_2$, in which the polaron state would reach and merge with the valence band. Figure 26b shows the polaron state below CBM versus U values. Experimentally, using ellipsometry on m-HfO$_2$ thin film, Takeuchi et al.[85] identified a broad absorption band lying about 1.2 eV below the conduction band, which might be intepreted as the polaron state below the conduction band.

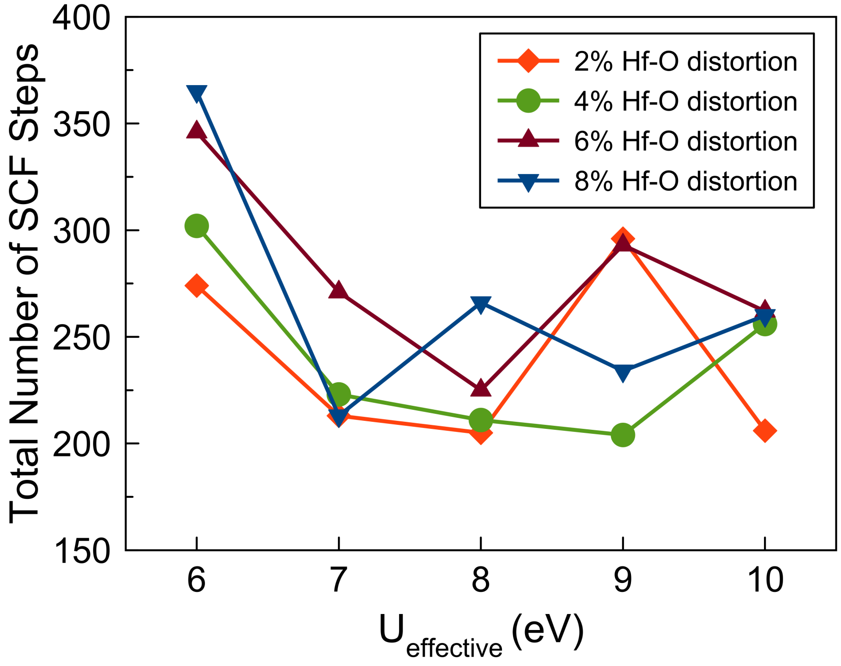

Figure 23: Total number of self consistent field (SCF) steps for cases where a polaron is formed

Figure 23 shows the total number of self-consistent field (SCF) steps needed to converge to a polaron solution with different initial distortions and different U values. We found that 2% and 4% Hf-O initial bond elongations generally gave the smallest number of SCF steps because they were closer to the average Hf-O bonds in the final polaron solutions (Figure 20). No general trend was found between the number of SCF steps with different U values being employed and with different initial % distortion.

4.2.3 Electron Attractor Method

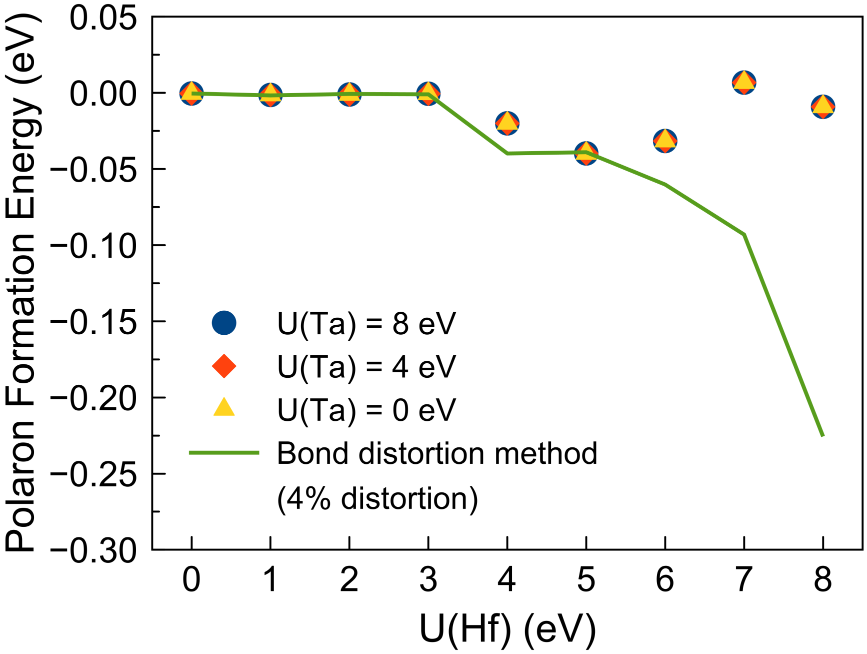

Figure 24: Polaron formation energy in m-HfO_2 using the electron attractor method. U(Hf) and U(Ta) represent the U values employed on Hf and Ta. Polaron formation energy data using the bond distortion method (4% distortion) is shown for comparison. No polarons formed using the electron attractor method for m-HfO_2. The tabulated polaron formation energy results using the electron atractor method are shown in the Appendix, Table A6.

To evaluate the electron attractor method for m-HfO_2, we substituted a Hf atom with a Ta atom, which has a more positive nucleus than the Hf atom. We employed a U value of 0, 4 and 8 eV on the Ta substituted atom, and a U value between 1 and 8 eV for the Hf atoms. The usage of different U values on Hf and Ta allowed us the assess various scenarious for polaron formation in m-HfO_2.

Figure 24 shows the polaron formation energy using different combinations of U(Hf) and U(Ta). We found that no polaron was formed using electron attractor method for m-HfO_2. This was unexpected since we found polaron formation in TiO_2 using the electron attractor method. To explain why no polaron was formed, we analyzed at the average Ta-O bond distortion for converged solution after replacing Hf with Ta, but before the substitute atom

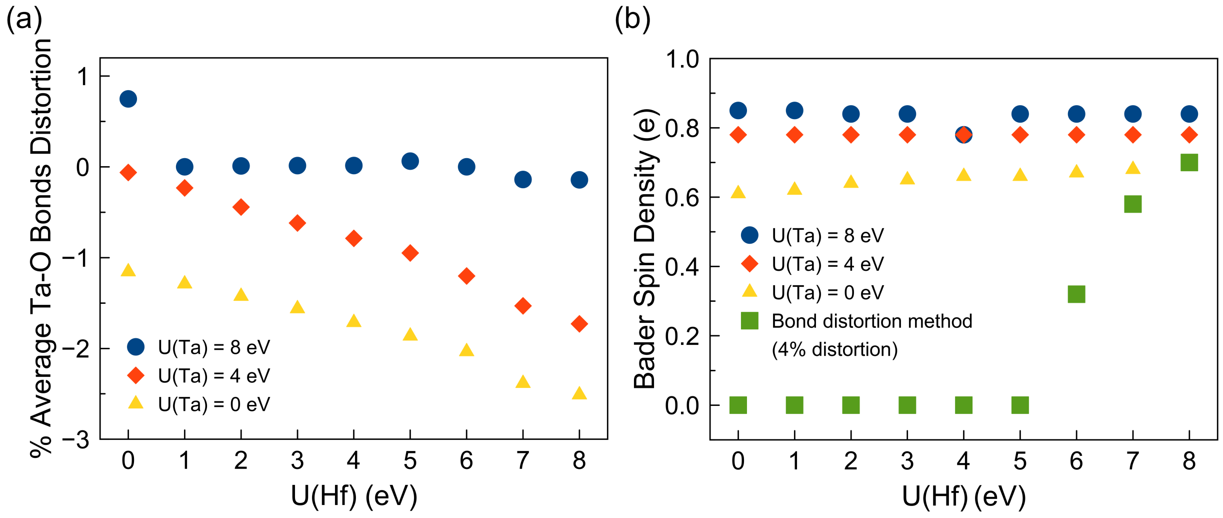

Figure 25: (a) Average Ta-O bond distortion compared to bulk m-HfO_2 for converged solution after replacing Hf with Ta, but before the substitute atom was removed and replaced by Hf at different U(Ta) and U(Hf) and (b) The Bader spin density of Ta for converged solution after replacing Ta with Hf, but before the substitute atom was removed and replaced by Hf.

was removed and replaced by Hf (Figure 25a). We saw that when a Hf atom was substituted with Ta, the bonds surrounding the polaron site were shortened, while polaron formation elongated Hf-O bonds (Figure 21). Therefore, Ta substitution gave an unfavorable starting geometry for polaron formation. We also looked that the Bader spin density of the Ta substitute atom. Figure 25b shows that Ta-replacement gives a reasonable starting charge density for m-HfO_2, since the unpaired electron was localized on the Ta site. Therefore, we concluded that electron attractor method using Ta substitution, though gave good initial guess for the charge density, failed to form a polaron because of the unfavorable starting geometry.

Another point on the TiO_2 electron attractor method that might explain the lack of polaron formation is that electron attractor method required a U(Ti) greater than the bond distortion method to form a polaron. For the bond distortion method in m-HfO_2, polarons only formed when $U(Hf) \geq 6eV$, while here we only used $U(Hf) \leq 8$ eV. Therefore, we suspected that increasing the U(Hf) in electron attractor method calculations might help facilitate polaron formation. We were also interested in testing electron attractor method using an with more positive nucleus, such as W. However, because of time limitation, we were not able to do so.

4.2.4 Polarons and Hybrid Functionals with m-HfO_2

Similar to previous TiO_2 work, we used the HSE06[68] hybrid functional to study polaron formation in m-HfO_2. To reduce the computational cost, we used the converged solutions (geometry and wavefunction) from GGA+U calculations (U = 6eV) and relaxed the structure using HSE06 functional. Converged polaron solution was obtained from bond distortion method using 4% Hf-O bond distortion and converged delocalized solution was from 0% distortion. We used both delocalized solution and polaron solution as the initial guess to see whether the polaron formation would depend on the initial guess in HSE06.

We found that HSE06 calculations always gave delocalized solutions for m-HfO_2, no matter whether we started from a converged polaron or delocalized solution from GGA+U. However, using B3LYP hybrid functionals, Ramo et al.[24] found a polaron solution lying 0.32 eV below the CBM. It should also be noted that Bradley et al.[86] tried to repeat this result from Ramo et al. using the HSE06 functional but did not succeed. Bradley et al. explained that because the polaron state was close to the conduction band minimum, and because HSE06 gave a smaller band gap than B3LYP, the narrower band gap might mean that the polaron state was covered by the conduction band in HSE06 calculation. Another important aspect is the percentage of Hatree-Fock exchange (%HF exchange) in hybrid functional calculation, since increasing the % of HF reduces the self-interaction error in DFT and thus favors polaron formation over delocalization. As shown earlier in the TiO_2 work, increasing the %HF exchange facilitated the polaron formation in anatase.[21] Therefore, we expect that hybrid calculations using a larger %HF exchange may allow polaron formation in m-HfO_2.

We also compared the band gap of m-HfO_2 at different U values (GGA+U) to HSE06 calculations and experiment in Figure 26a. Pure PBE predicted the band gap of m-HfO_2 to be 4.2 eV, significantly underestimated compared to the experimental band gap of 5.7 eV.[85]

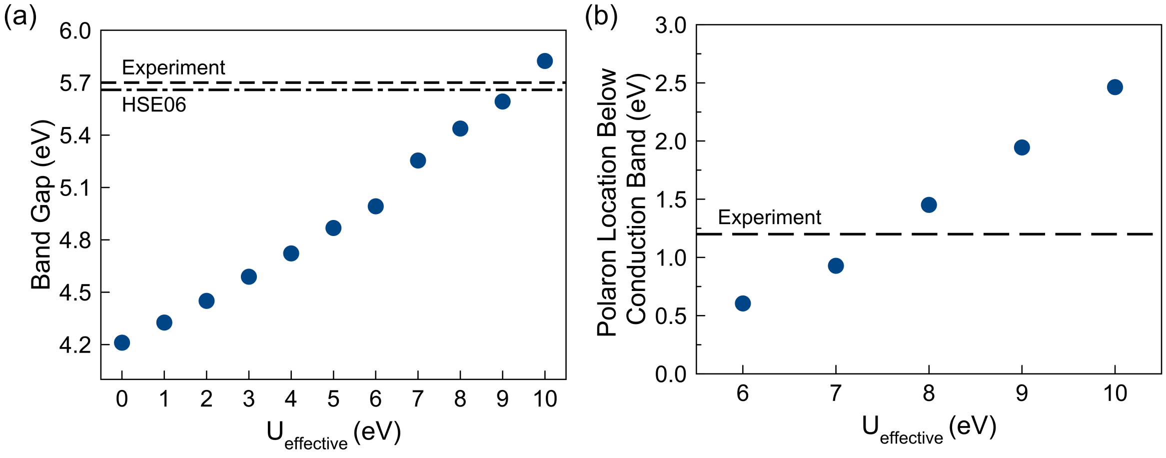

Figure 26: (a) m-HfO_2 band gaps versus $U_{effective}$ compared with HSE06 and experiment.[85] (b) Polaron state location for GGA+U results and experiment.[85] No polaron formed for m-HfO_2 using the HSE06 functional.

Using a U value of about 9 eV, we can obtain the experimental band gap of m-HfO_2. HSE06, on the other hand, predicted a band gap of 5.66 eV, in good agreement with experimental results.

To summarize, we showed that HSE06 did not predict polaron formation in m-HfO_2. On the other hand, by tuning the U value, GGA+U was able to obtain the experimental polaron state below the conduction band. We also noted that by increasing the % HF exchange, we might be able to obtain polaron structure.

4.3 $BiVO_4$

4.3.1 Sample polarons in $BiVO_4$

Similar to previous polaron calculations with rutile, anatase, and m-HfO_2, we verified that polarons formed in m-$BiVO_4$. We examined the spin density to confirm if there was electron localization. Figure 27 shows the spin density around a polaronic V atom. The Bader charge of a V polaron site was 2.1 - 2.3, while non-polaron V atoms had charges of 2.2-2.3. The Bader spin charge of a V polaron site was 0.9e - 1.1e and of a non-polaron site was 0.1e - 0.2e. We noted that Bader charge was not particularly helpful in discerning polaron formation in

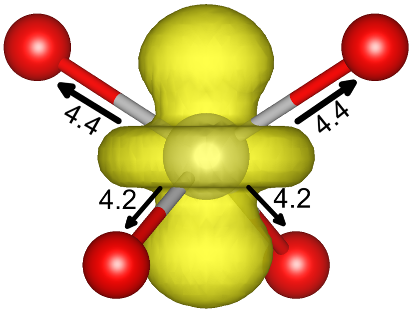

Figure 27: Example polarons formed in m-$BiVO_4$ using 4% V-O bond distortion. Shown is the spin density around the polaronic V site. The numbers show the % that the V-O bonds increased upon polaron formation. Grey spheres are V and red spheres are O.

m-$BiVO_4$ since the difference between the charge of a polaron site and a non-polaron site was about 0.1e. Secondly, we checked if there were lattice distortions surrounding the polaron site compared to the neutral m-$BiVO_4$ bulk to confirm polaron formation.

4.3.2 Bond Distortion Method

Figure 28 shows that without initial V-O bond distortions (0% V-O bonds distortion), no polaron was formed no matter what U value was applied. We saw that when a polaron was formed, 2%, 4%, 6% and 8% distortions always converged to the same polaron solution. This result was more consistent than in TiO_2 and m-HfO_2, because in TiO_2 calculations, at certain U values, 2% distortion did not form polaron and in m-HfO_2, certain combinations of intia; % distortion and U value did not form polaron. We found that a polaron was formed with $U \geq 2$ eV (Figure 28. Similar to results with TiO_2 and m-HfO_2, we found that as the U value increased, the polaron structure became more stable than the delocalized structure.

Figure 29 shows the average, minimum and maximum V-O bond elongations upon polaron formation. Unlike TiO_2 and m-HfO_2, the distortions of the four V-O bonds surrounding the V polaronic site were all very similar, indicating the polaron was more symmetric than other polarons. These average, minimum and miximum V-O bond elongations increased as U values increased, and reached a common value of about 5.2%.

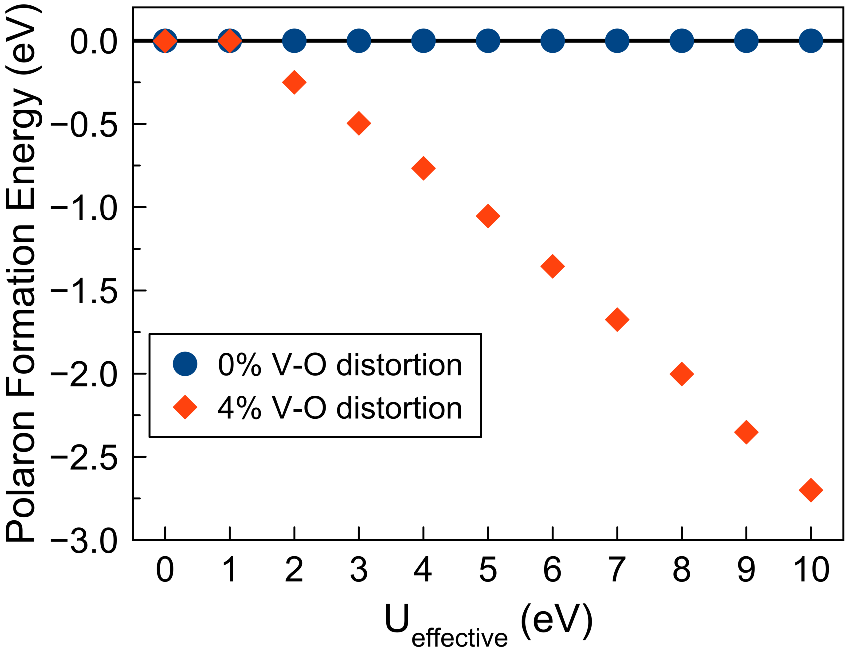

Figure 28: Polaron formation energies in m-BiVO$_4$ using 0% and 4% initial V-O bond distortions versus U$_{effective}$. A full listing of polaron formation energies using different intial % distortions is shown in the Appendix, Table A7.

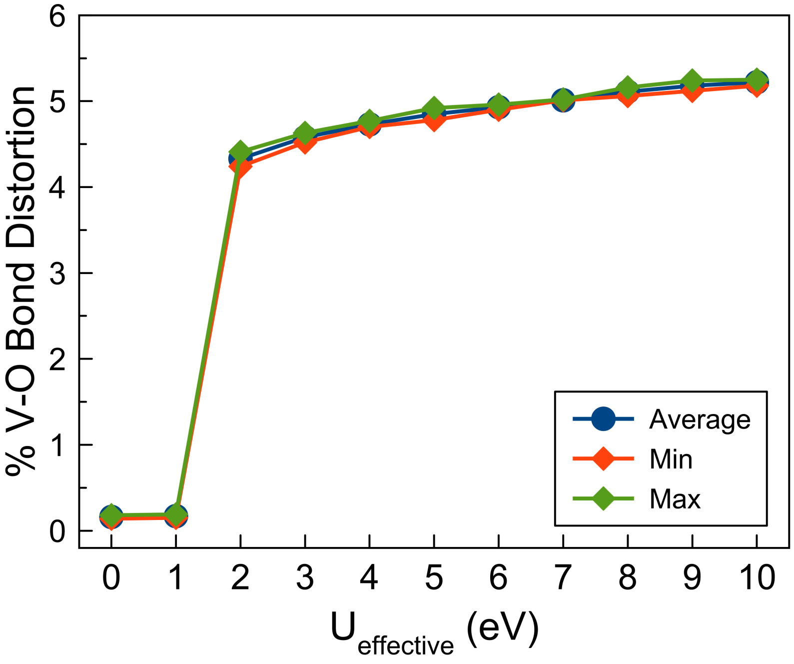

Figure 29: Average, minimum and maximum V-O bond distorations for polaron solutions at different U values using an initial 4% distortion.

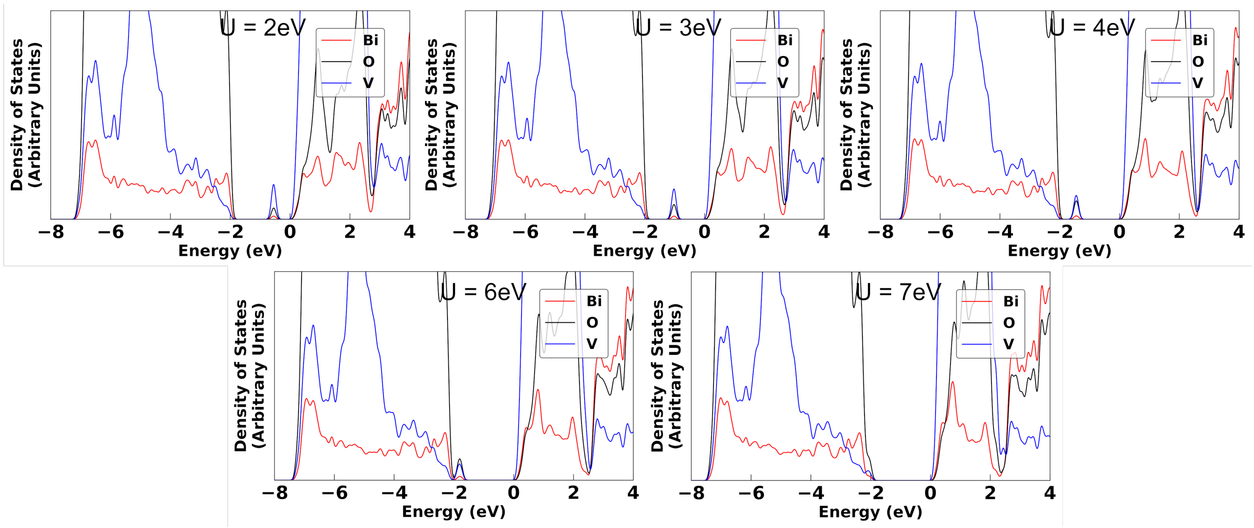

Figure 30: Projected density of states for m-BiVO$_4$ using different U values where a polaron formed. The zero energy was chosen as the conduction band minimum (CBM). The polaron exists as a small gap state predominantly on V atoms. At U values of 7 eV and greater, the polaron state was completely within the valence band.

We also analyzed the electronic properties of m-$BiVO_4$ structures where polarons formed. Figure 30 shows the projected density of state for m-$BiVO_4$ for calculations with U = 2-7 eV. At, higher U values (U = 8-10 eV), the polaron state was completely within the valence band, so are not shown in the graph. Similar to TiO_2 and m-HfO_2 results, we saw that when the polaron formed at low U values (U = 2 eV), the polaron state is located near the conduction band minimum. As the U value increased, the polaron state shifted toward the valence band before completely merging with the valence band at around U = 7 eV.

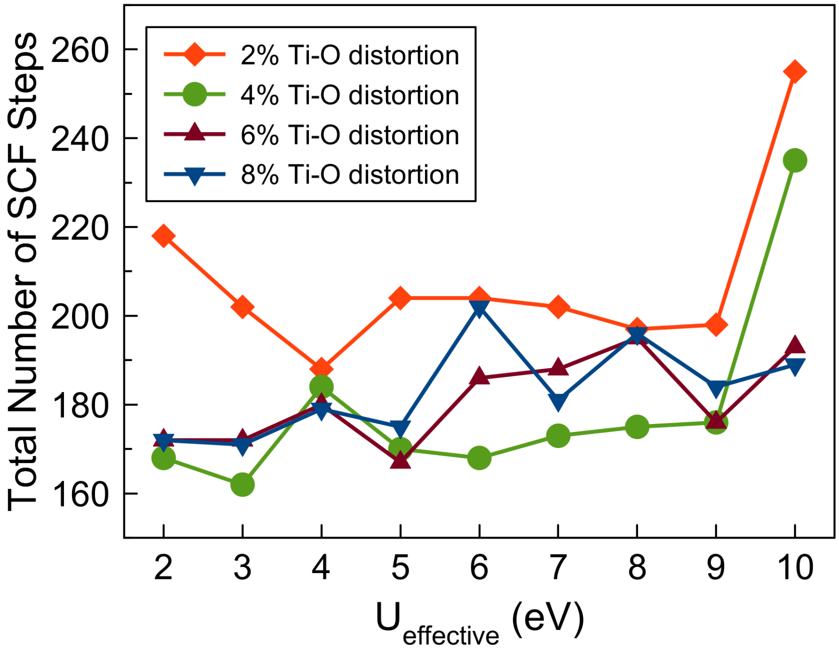

Figure 31: Total number of self consistent field (SCF) steps needed for convergence for the cases when a polaron formed in m-$BiVO_4$.

To determine which initial % distortion allowed the quickest polaron formation, we compared the total number of SCF steps between each % distortion (Figure 31). The total number of SCF steps was summed up from all the geometry steps. We saw that for $U \leq 8$ eV, inital 4% distortion structures in general converged the fastest. This was due to the similarity between the starting geometry with 4% distortion and the polaron structure, as shown in Figure 29. For $U \geq 9eV$, 6% distortion started to converge faster the 4%, becaues the final bbond distortion of the polaron structures at these U values were closer to 6% than 4%.

To conclude, for m-$BiVO_4$, we saw that when a polaron was formed 2, 4, 6 and 8% gave the same polaron solutions. With regard to convergence speed, 4% and 6% initial distortions generally outperformed the 2% and 8% distortions due to their close resemblance to the actual polaron solutions.

4.3.3 Electron Attractor Method

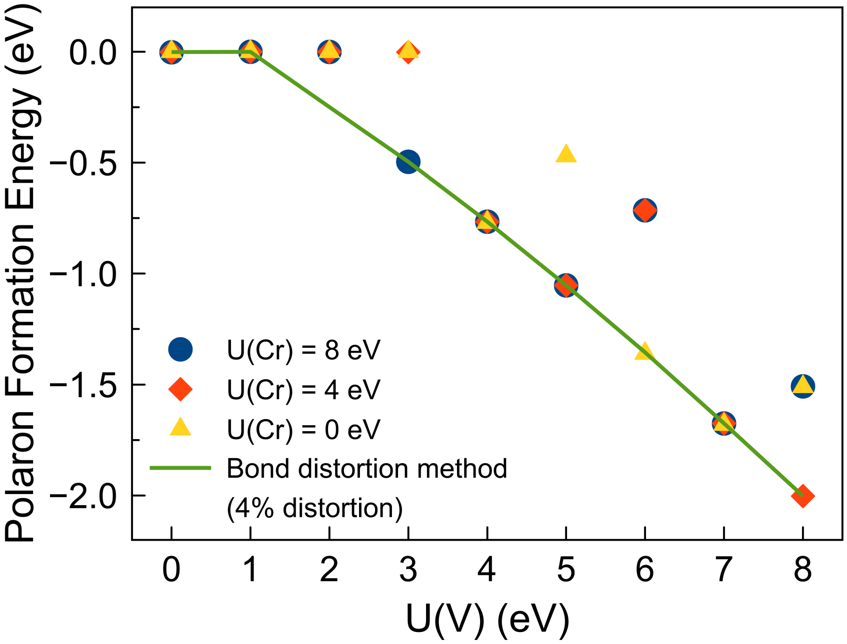

Figure 32: Polaron formation energy in (m-$BiVO_4$ using the electron attractor method where a V atom is replaced by Cr to create initial geometries/wavefunctions. U(V) and U(Cr) represent the U values employed on V and Cr, respectively. Results from the bond distortion method (4% distortion) are also shown for comparison. The complete results are shown in the Appendix, Table A8).

Figure 32 shows the polaron formation energies employed on V was larger than that in bond distortion method ($U(V) \geq 2$ eV to form polaron). Moreover, we also found that electron attractor method frequently gave meta-stable polaron structures, in which the unpaired electron was not localized on a single V atom as in the bond distortion method, but was localized on two neighboring V sites, as shown in Figure 33. These meta-stable polaron structures were about 0.5 eV less stable than the most stable polaron solutions (when the electron was localized on a single V atom).

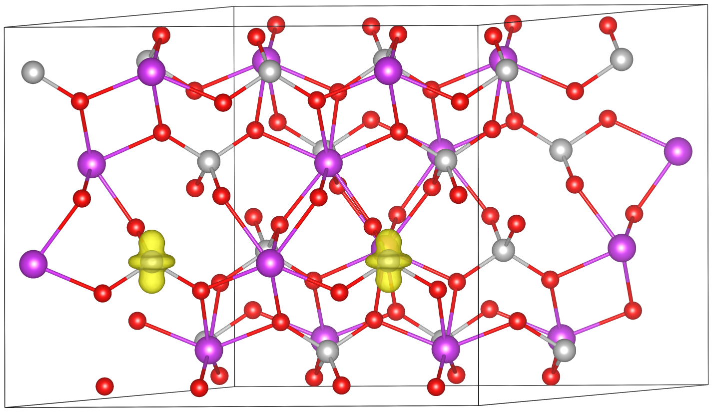

Figure 33: A meta-stable polaron structure obtained from the electron attractor method, in which the electron is localized on two neighboring V atoms. The spin density results are shown for the case of U(V) = U(Ti) = 8eV. Grey spheres are V, red spheres are O and purple spheres are Bi.

To understand why using the electron attractor method polaron formation required a larger U(V) than the bond distortion method, and why meta-stable polaron structures were found using electron attractor method, we analyzed the average Cr-O bond distortion for converged solution after replacing V with Cr, but before the substitute atom was removed and replaced by V (Figure 34a) and the Bader spin density of Cr for converged solutions after replacing V with Cr (Figure 34b). Figure 34a shows that when U(Cr) = 0 and 4 eV, Cr-O bonds were always shortened, leading to unfavorable structures for polaron formation since polaron formation would elongate V-O bonds. Using U(Cr) = 8 eV elongated Cr-O bonds for $U(V) \leq 6$ eV. Figure 34b shows that using U(Cr) = 8 eV overestimated the Bader spin density of the polaron site, while U(Cr) = 0 and 4 eV gave a spin density close to actual

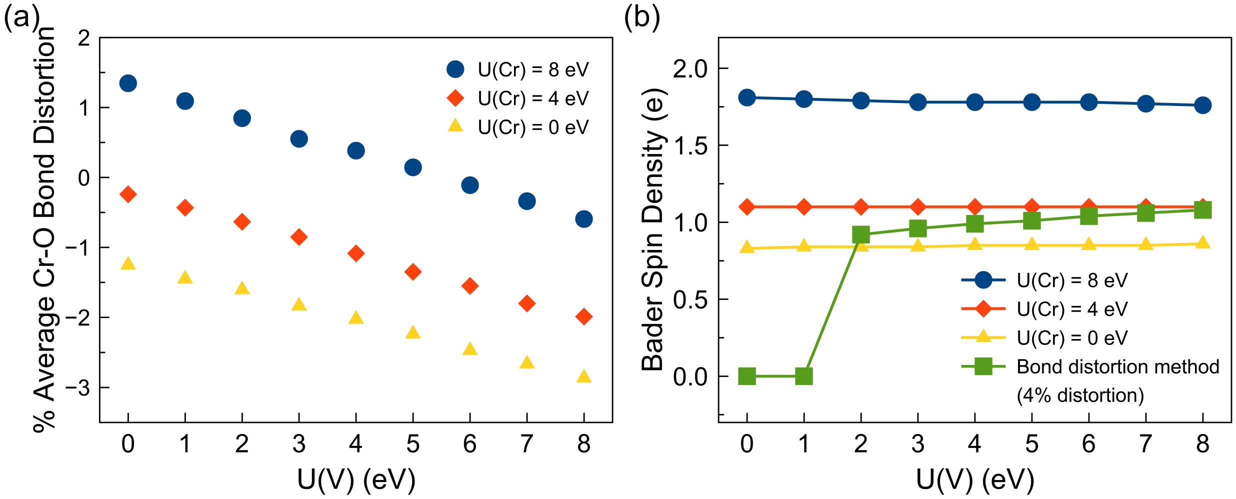

Figure 34: (a) Average Cr-O bond distortions compared to bulk m-$BiVO_4$ for converged solutions after replacing V with Cr, but before the substitute atom was removed and replaced by V and (b) The Bader spin charges of Cr for converged solution after replacing V with Cr, but before the substitute atom was removed and replaced by V.

polaron formation. From these results, we could conclude that both initial geometries and wavefunctions were important to converge to the most stable polaron solution.

Figure 35 shows that the total number of SCF steps using the bond distortion method (4% disotrtion) was significantly smaller than using the electron attractor method. Similar to the TiO_2 results, we believe that the bond distortion method converged faster than electron attractor method because of the similarity between bond distortion initial geometry and actual polaron solution (Figure 29. On the contrary, the electron attractor method gave an unfavorable starting geometry for polaron formation by shortening the V-O bonds and thus converged slower.

4.3.4 Polarons and Hybrid Functionals with m-$BiVO_4$

Similar to calculations with TiO_2 and m-HfO_2, we employed the HSE06[68] hybrid functional to study polaron formation in m-$BiVO_4$. We used previously converged GGA+U results (geometry and wavefunction) as the initial guesses and then relaxed the systems using HSE06 functional. We started with both polaron and delocalized solutions from GGA+U to see if

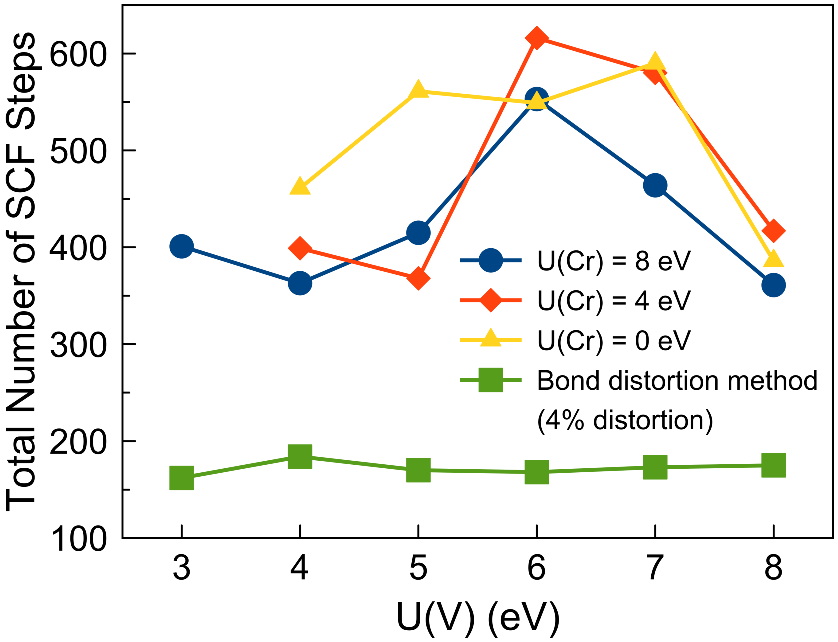

Figure 35: The total number of SCF steps for calculations in which polarons formed using the electron attractor method for m-BiVO$_4$. Data from the bond distortion method (4% distortion) is shown for comparison. A tabulated results is shown in the Appendix, Table A8.

polaron formation depended on the initial geometry and wavefunction.

We found that a polaron was formed only when we started with a polaron solution as the initial guess. A delocalized solution was found when we started with a delocalized guess. The polaron formation energy was -0.83 eV, which is equivalent to calculation obtained from GGA+U using $U \sim 4$ eV. The polaron Bader charge was 2.1 e- and the Bader spin charge value was 0.94 e-. The polaron state was about 2.49 eV below the conduction band (Figure 36b). A similar polaron location in m-BiVO$_4$ was obtain by Kweon et al.,[22] in which a polaron was found to lie about 2.4 eV below the conduction band minimum. Using the dielectric-dependent hybrid (DDH) functional, Seo et al.[87] predicted a polaron location of 1.79 eV below the conduction band. To the best of our knowledge, there has been no experimental data to verify the electron level below the conduction band of m-BiVO$_4$. As a result, no conclusion could be drawn about the accuracy of modeling polaron using GGA+U and HSE06.

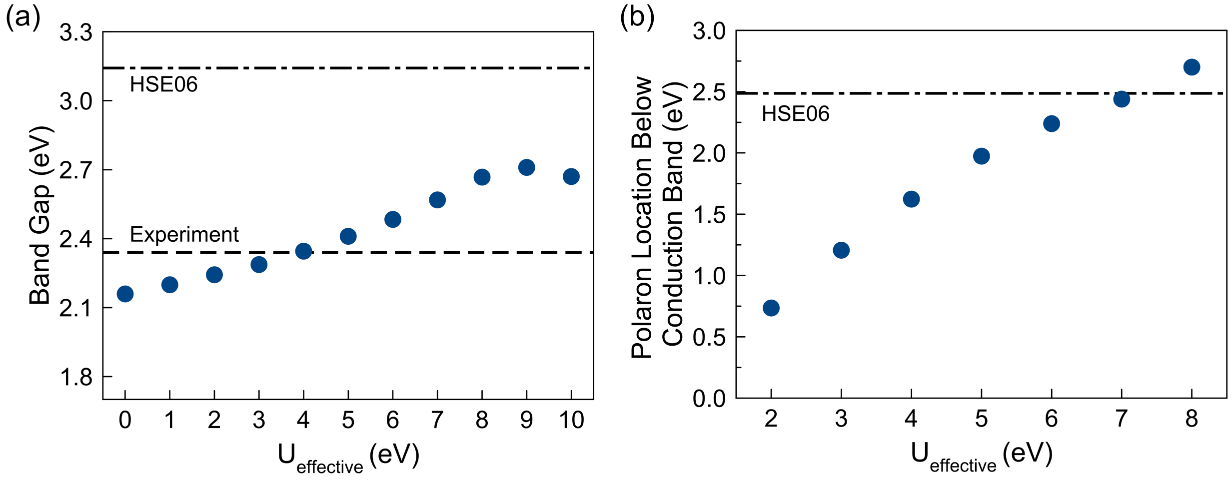

Figure 36: (a) m-BiVO$_4$ band gap versus U$_{effective}$ compared with HSE06 and experimental results.(b) Polaron state below the CBM for GGA+U and HSE06 results. The experimental band gap for m-BiVO$_4$ is about 2.34 eV, and was obtained from Tokunaga et al.[88]

We also compared the band gap of m-BiVO$_4$ using GGA, GGA+U and HSE06 and experimental results. Experimentally, the band gap of m-BiVO$_4$ was found to be 2.34 eV.[88] We found that GGA underestimated the band gap by about 0.3 eV. Similar band gap underestimation using GGA was obtained by Saker et al.[67] By increasing U value, we obtained the experimental band gap of m-$BiVO_4$ at U = 4 eV. HSE06 significantly overestimated the band gap, predicting the band gap value of 3.1 eV. Similar band gap overestimation was observed by Kweon et al.,[22] who showed that using 25% HF exchange gave a band gap of 3.5 eV.

5 Conclusions

We modeled electron polaron formation in four different metal oxides: TiO_2 rutile, TiO_2 anatase, m-HfO_2 and m-$BiVO_4$. We employed two methods to model polaron, bond distortion method and electron attractor method. To overcome the self-interaction error in Density Functional Theory, we used two types of correction, Hubbard correction and hybrid functionals.

We showed that to form polaron, an initial distortion surrounding the polaron site must be introduced to the bulk structure accompanied with Hubbard correction (U values). We found that the U value employed significantly affected the polaron formation. To form polaron, the U values employed must be equal or greater than 3 eV, 4eV, 6 eV and 2 eV for TiO_2 rutile, TiO_2 anatase, m-HfO_2 and m-$BiVO_4$ were 3 eV, 4eV, 6 eV and 2 eV, respectively. At U values closer to these cutoffs, electron might be localized on several polaronic site instead of a single polaronic site, such as in m-HfO_2. As the U value increased, the electron became completely localized on a single site. We also found that for each material, as the U value increased, the spatial extention of the polaron, or the lattice distortion surrounding the polaron site increased and reached a common value.

Using bond distortion method, with different U value, we found that a certain level of distortion must be introduced to form a polaron. For instance, at U = 3 eV in rutile, 2% bond distortion resulted in no polaron formation while 4, 6 and 8% distortion gave polaron structure. When a polaron structure formed, different initial structures converged to the same polaron solution. In general, using 4% initial distortion allowed the polaron structure to converge the fastest. We found no significant trend between the speed of calculation in terms of the number of self-consistent field steps and the initial % distortion and the U value.

Using electron attractor method, we tested two substitute atoms in TiO_2 calculations (V and Cr) but only tested one substitute atom for m-HfO_2 (Ta) and m-$BiVO_4$ (Cr) because of time limitation. We found that electron attractor method required a larger U cutoff than bond distortion method to form polaron. Electron attractor method attracted allowed better starting charge density be attracting the electron to a substitute atom site, but in most cases it shortened the bond surrounding that site. Since polaron formation elongated bonds surrounding the polaron site, electron attractor method gave a poor starting geometry for polaron calculations. The poor starting geometry might result in no polaron formation or meta-stable polaron structure. We also found that the convergence with electron attractor was slower than bond distortion method due to the poor prediction of polaron structure. Therefore, based on the accuracy and speed of polaron calculations, we would recommend the bond distortion method over electron attractor method to model polaron in metal oxides.

In hybrid functional (HSE06) calculations, we found polaron formation only in TiO_2 rutile and m-$BiVO_4$. We saw that starting from converged polaron structure with GGA+U might form a polaron (TiO_2 rutile and m-$BiVO_4$) or a delocalized solution (TiO_2 anatase and m-Hfo_2). Starting from a delocalized solution from GGA+U, we always obtained delocalized solution. Studying the electronic structure of polaron, we found that by tuning the U values, we were able to obtain the experimental polaron state within the band gap in TiO_2 rutile and anatase, and m-HfO_2. HSE06 slightly overestimated the polaron state below conduction band in TiO_2 rutile. We noted that by increasing the % Hartree-Fock exchange and increasing the modeled supercell, we might be able to obtain polaron formation with hybrid functional, as such methods were conducted to form polaron in TiO_2 anatase.[21] We also looked at the band gap prediction of GGA+U and HSE06 in comparison to experimental values. By tuning the U value, GGA+U could obtain the experimental band gap for all four materials.

HSE06 overestimated the band gap, slightly in TiO_2 rutile and anatase, and significantly in m-$BiVO_4$. HSE06 gave good band gap prediction for m-HfO_2. We also noted that HSE06 was significantly more computational expensive and GGA+U calculation.

In conclusion, we found that using bond distortion method with 4% initial distortion was generally ideal for all the studied materials. The degree of Hubbard correction (U value) was significantly important for polaron formation. In modeling polaron, the U value in GGA+U might be tuned to fit experimental measurement of polaron state within the band. HSE06 was able to form polaron in certain materials, but a larger supercell might be needed to form polaron for other materials.

Acknowledgement

The authors would like to acknowledge the Academic & Research Computing group at Worcester Polytechnic Institute for providing support that contributed to the results reported within this MQP. The authors also thank the graduate students in Professor Deskins research group (Lida Farsi and Tao Yan) for assisting with this research.

References

(1) Nomura, K.; Ohta, H.; Takagi, A.; Kamiya, T.; Hirano, M.; Hosono, H. *Nature* **2004**, *432*, 488.

(2) Delbeke, D.; Bockstaele, R.; Bienstman, P.; Baets, R.; Benisty, H. *IEEE Journal of Selected Topics in Quantum Electronics* **2002**, *8*, 189–206.

(3) Park, J. S.; Maeng, W.-J.; Kim, H.-S.; Park, J.-S. *Thin solid films* **2012**, *520*, 1679–1693.

(4) Su, J.; Guo, L.; Bao, N.; Grimes, C. A. *Nano letters* **2011**, *11*, 1928–1933.

(5) Guo, C. X.; Yang, H. B.; Sheng, Z. M.; Lu, Z. S.; Song, Q. L.; Li, C. M. *Angewandte Chemie International Edition* **2010**, *49*, 3014–3017.

(6) Tilley, S. D.; Cornuz, M.; Sivula, K.; Grätzel, M. *Angewandte Chemie International Edition* **2010**, *49*, 6405–6408.

(7) Sivula, K.; LeFormal, F.; Grtzel, M. *ChemSusChem* **2011**, *4*, 432–449.

(8) Lin, Y.; Li, Y.; Zhan, X. *Chemical Society Reviews* **2012**, *41*, 4245–4272.

(9) others,, et al. *Advanced optical materials* **2015**, *3*, 147–164.

(10) Hoffmann, M. R.; Martin, S. T.; Choi, W.; Bahnemann, D. W. *Chemical reviews* **1995**, *95*, 69–96.

(11) Hashimoto, K.; Irie, H.; Fujishima, A. *Japanese journal of applied physics* **2005**, *44*, 8269.

(12) Fox, M. A.; Dulay, M. T. *Chemical reviews* **1993**, *93*, 341–357.

(13) Alexandrov, A. S. *Polarons in Advanced Materials*, 1st ed.; Springer: Dordrecht, The Netherlands, 2007.

(14) Devreese, J. T. *Encycl. Appl. Phys.* **1996**, *14*, 383–409.

(15) Austin, I. G.; Mott, N. F. *Advances in Physics* **2001**, *50*, 757–812.

(16) Rettie, A. J.; Chemelewski, W. D.; Emin, D.; Mullins, C. B. *The journal of physical chemistry letters* **2016**, *7*, 471–479.

(17) others,, et al. *Physical Review B* **2013**, *87*, 125201.

(18) Ziwritsch, M.; Muller, S.; Hempel, H.; Unold, T.; Abdi, F. F.; van de Krol, R.; Friedrich, D.; Eichberger, R. *ACS Energy Letters* **2016**, *1*, 888–894.

(19) Deskins, N. A.; Dupuis, M. *Physical Review B* **2007**, *75*, 195212.

(20) Setvin, M.; Franchini, C.; Hao, X.; Schmid, M.; Janotti, A.; Kaltak, M.; Van de Walle, C. G.; Kresse, G.; Diebold, U. *Physical review letters* **2014**, *113*, 086402.

(21) Spreafico, C.; VandeVondele, J. *Physical Chemistry Chemical Physics* **2014**, *16*, 26144–26152.

(22) Kweon, K. E.; Hwang, G. S.; Kim, J.; Kim, S.; Kim, S. *Physical Chemistry Chemical Physics* **2015**, *17*, 256–260.

(23) Kweon, K. E.; Hwang, G. S. *Physical Review B* **2013**, *87*, 205202.

(24) Ramo, D. M.; Shluger, A.; Gavartin, J.; Bersuker, G. *Physical review letters* **2007**, *99*, 155504.

(25) Chretien, S.; Metiu, H. *The Journal of Physical Chemistry C* **2011**, *115*, 4696–4705.

(26) Dudarev, S.; Botton, G.; Savrasov, S.; Humphreys, C.; Sutton, A. *Physical Review B* **1998**, *57*, 1505.

(27) Anisimov, V. I.; Aryasetiawan, F.; Lichtenstein, A. *Journal of Physics: Condensed Matter* **1997**, *9*, 767.

(28) Liechtenstein, A.; Anisimov, V.; Zaanen, J. *Physical Review B* **1995**, *52*, R5467.

(29) Fujishima, A.; Honda, K. *nature* **1972**, *238*, 37.

(30) Martin, D. J.; Qiu, K.; Shevlin, S. A.; Handoko, A. D.; Chen, X.; Guo, Z.; Tang, J. *Angewandte Chemie International Edition* **2014**, *53*, 9240–9245.

(31) Karunakaran, C.; Senthilvelan, S. *Electrochemistry Communications* **2006**, *8*, 95–101.

(32) Tsuda, N.; Nasu, K.; Yanase, A.; Siratori, K. *Electronic Conduction in Oxides*; Springer, 1991; pp 1–4.

(33) Park, Y.; McDonald, K. J.; Choi, K.-S. *Chemical Society Reviews* **2013**, *42*, 2321–2337.

(34) Fujishima, A.; Rao, T. N.; Tryk, D. A. *Journal of photochemistry and photobiology C: Photochemistry reviews* **2000**, *1*, 1–21.

(35) Fujishima, A.; Zhang, X.; Tryk, D. A. *Surface science reports* **2008**, *63*, 515–582.

(36) Xi, G.; Ye, J. *Chemical Communications* **2010**, *46*, 1893–1895.

(37) Fan, H.; Jiang, T.; Li, H.; Wang, D.; Wang, L.; Zhai, J.; He, D.; Wang, P.; Xie, T. *The Journal of Physical Chemistry C* **2012**, *116*, 2425–2430.

(38) Xi, L.; Chiam, S. Y.; Mak, W. F.; Tran, P. D.; Barber, J.; Loo, S. C. J.; Wong, L. H. *Chemical Science* **2013**, *4*, 164–169.

(39) Kim, J. Y.; Magesh, G.; Youn, D. H.; Jang, J.-W.; Kubota, J.; Domen, K.; Lee, J. S. *Scientific reports* **2013**, *3*, 2681.

(40) Wang, D.; Wang, Q.; Javey, A.; Tu, R.; Dai, H.; Kim, H.; McIntyre, P. C.; Krishnamohan, T.; Saraswat, K. C. *Applied Physics Letters* **2003**, *83*, 2432–2434.

(41) Ahn, K. Y.; Forbes, L. Atomic layer deposited nanolaminates of HfO2/ZrO2 films as gate dielectrics. 2005; US Patent 6,921,702.

(42) Wang, Z.; Yu, H.; Tran, X. A.; Fang, Z.; Wang, J.; Su, H. *Physical review B* **2012**, *85*, 195322.

(43) Cheng, Y.; Zhu, L.; Ying, Y.; Zhou, J.; Sun, Z. *Applied Surface Science* **2018**, *447*, 618–626.

(44) Liu, T.; Zhou, X.; Dupuis, M.; Li, C. *Physical Chemistry Chemical Physics* **2015**, *17*, 23503–23510.

(45) Foster, A. S.; Gejo, F. L.; Shluger, A.; Nieminen, R. M. *Physical Review B* **2002**, *65*, 174117.

(46) Lazzeri, M.; Vittadini, A.; Selloni, A. *Physical Review B* **2001**, *63*, 155409.

(47) others,, et al. *Science* **2017**, *357*, 898–903.

(48) Kohn, W.; Sham, L. J. *Phys. Rev.* **1965**, *140*, A1133–A1138.

(49) Perdew, J. P.; Burke, K.; Ernzerhof, M. *Physical review letters* **1996**, *77*, 3865.

(50) Cramer, C. J.; Truhlar, D. G. *Physical Chemistry Chemical Physics* **2009**, *11*, 10757–10816.

(51) Li, J.; Meng, S.; Li, L.; Lu, H.; Tohyama, T. *Computational Materials Science* **2014**, *81*, 397–401.

(52) Sholl, D.; Steckel, J. A. *Density functional theory: a practical introduction*; John Wiley & Sons, 2011.

(53) Lewars, E. G. *Computational Chemistry: Introduction to the Theory and Applications of Molecular and Quantum Mechanics*, 2nd ed.; Springer: Cambridge, United Kingdom, 2011.

(54) Kresse, G.; Hafner, J. *Physical Review B* **1993**, *47*, 558.

(55) Kresse, G.; Hafner, J. *Physical Review B* **1994**, *49*, 14251.

(56) Kresse, G.; Furthmüller, J. *Computational materials science* **1996**, *6*, 15–50.

(57) Kresse, G.; Furthmüller, J. *Physical review B* **1996**, *54*, 11169.

(58) Walsh, A.; Yan, Y.; Huda, M. N.; Al-Jassim, M. M.; Wei, S.-H. *Chemistry of Materials* **2009**, *21*, 547–551.

(59) Kresse, G.; Joubert, D. *Physical Review B* **1999**, *59*, 1758.

(60) Blöchl, P. E. *Physical review B* **1994**, *50*, 17953.

(61) Morgan, B. J.; Watson, G. W. *Surface Science* **2007**, *601*, 5034–5041.

(62) Murnaghan, F. *Proceedings of the national academy of sciences of the United States of America* **1944**, *30*, 244.

(63) Stacy, D. W.; Johnstone, J. K.; Wilder, D. *Journal of the American Ceramic Society* **1972**, *55*, 482–483.

(64) Adam, J.; Rogers, M. *Acta Crystallographica* **1959**, *12*, 951–951.

(65) Jaffe, J. E.; Bachorz, R. A.; Gutowski, M. *Physical Review B* **2005**, *72*, 144107.

(66) Zhao, X.; Vanderbilt, D. *Physical Review B* **2002**, *65*, 233106.

(67) Sarker, H. P.; Rao, P. M.; Huda, M. N. *ChemPhysChem* **2019**, *20*, 773–784.

(68) Heyd, J.; Scuseria, G. E.; Ernzerhof, M. *The Journal of chemical physics* **2003**, *118*, 8207–8215.

(69) Krukau, A. V.; Vydrov, O. A.; Izmaylov, A. F.; Scuseria, G. E. *The Journal of chemical physics* **2006**, *125*, 224106.

(70) Hutchinson, M.; Widom, M. *Computer Physics Communications* **2012**, *183*, 1422–1426.

(71) Hacene, M.; Anciaux-Sedrakian, A.; Rozanska, X.; Klahr, D.; Guignon, T.; Fleurat-Lessard, P. *Journal of computational chemistry* **2012**, *33*, 2581–2589.

(72) Maintz, S.; Eck, B.; Dronskowski, R. *Computer Physics Communications* **2011**, *182*, 1421–1427.

(73) Walker, R. C.; Goetz, A. W. *Electronic Structure Calculations on Graphics Processing Units: From Quantum Chemistry to Condensed Matter Physics*; John Wiley & Sons, 2016.

(74) Iyemperumal, S. K.; Pham, T. D.; Bauer, J.; Deskins, N. A. *The Journal of Physical Chemistry C* **2018**, *122*, 25274–25289.

(75) Shibuya, T.; Yasuoka, K.; Mirbt, S.; Sanyal, B. *Journal of Physics: Condensed Matter* **2012**, *24*, 435504.

(76) Wang, Z.; Bevan, K. H. *Physical Review B* **2016**, *93*, 024303.

(77) Janotti, A.; Franchini, C.; Varley, J.; Kresse, G.; Van de Walle, C. *physica status solidi (RRL)–Rapid Research Letters* **2013**, *7*, 199–203.

(78) Bader, R. *A Quantum Theory* **1990**,

(79) Henkelman, G.; Arnaldsson, A.; Jónsson, H. *Computational Materials Science* **2006**, *36*, 354–360.

(80) Tang, W.; Sanville, E.; Henkelman, G. *Journal of Physics: Condensed Matter* **2009**, *21*, 084204.

(81) Sanville, E.; Kenny, S. D.; Smith, R.; Henkelman, G. *Journal of computational chemistry* **2007**, *28*, 899–908.

(82) Deák, P.; Aradi, B.; Frauenheim, T. *Physical Review B* **2011**, *83*, 155207.

(83) Tang, H.; Berger, H.; Schmid, P.; Levy, F.; Burri, G. *Solid State Communications* **1993**, *87*, 847–850.

(84) Pascual, J.; Camassel, J.; Mathieu, H. *Physical Review B* **1978**, *18*, 5606.

(85) Takeuchi, H.; Ha, D.; King, T.-J. *Journal of Vacuum Science & Technology A: Vacuum, Surfaces, and Films* **2004**, *22*, 1337–1341.

(86) Bradley, S. R. Computational Modelling of Oxygen Defects and Interfaces in Monoclinic HfO2. Ph.D. thesis, UCL (University College London), 2016.

(87) Seo, H.; Ping, Y.; Galli, G. *Chemistry of Materials* **2018**, *30*, 7793–7802.

(88) Tokunaga, S.; Kato, H.; Kudo, A. *Chemistry of Materials* **2001**, *13*, 4624–4628.

Appendix

Thang Duc Pham and N. Aaron Deskins*

Department of Chemical Engineering, Worcester Polytechnic Institute, Worcester, MA

E-mail: nadeskins@wpi.edu

1 TiO_2

1.1 Bond distortion method

Table A1: Polaron formation energy in eV for TiO_2 rutile at different U values and different initial %distortion. A negative value shows that a polaron is formed is formed. Non-negative value indicates that no polaron is formed

% Ti-O bond distortion	$U_{effective}$ (eV)										
	1	2	3	4	5	6	7	8	9	10	
0	0.00	0.00	0.00	0.00	0.00	0.00	0.00	0.00	0.00	0.00	0.00
2	0.00	0.00	0.00	0.00	-0.29	-0.56	-0.83	-1.12	-1.42	-1.73	-2.05
4	0.00	0.00	0.00	-0.07	-0.29	-0.56	-0.83	-1.12	-1.42	-1.73	-2.05
6	0.00	0.00	0.00	-0.07	-0.29	-0.55	-0.83	-1.12	-1.42	-1.73	-2.05
8	0.00	0.00	0.00	-0.07	-0.29	-0.56	-0.83	-1.12	-1.42	-1.73	-2.05

Table A2: Polaron formation energy in eV for TiO_2 rutile at different U values and different initial %distortion. A negative value and values with indicated mean that a polaron is formed. Non-negative value indicates that no polaron is formed.

% Ti-O bond distortion	$U_{effective}$ (eV)										
	0	1	2	3	4	5	6	7	8	9	10
0	0.00	0.00	0.00	0.00	0.00	0.00	0.00	0.00	0.00	0.00	0.00
2	0.00	0.00	0.00	0.00	0.00	-0.25	-0.53	-0.84	-1.16	-1.50	-1.86
4	0.00	0.00	0.00	0.00	-0.01	-0.25	-0.53	-0.84	-1.16	-1.50	-1.86
6	0.00	0.00	0.00	0.00	0.00*	-0.25	-0.53	-0.84	-1.16	-1.50	-1.86
8	0.00	0.00	0.00	0.00	0.00*	-0.25	-0.53	-0.84	-1.16	-1.50	-1.86

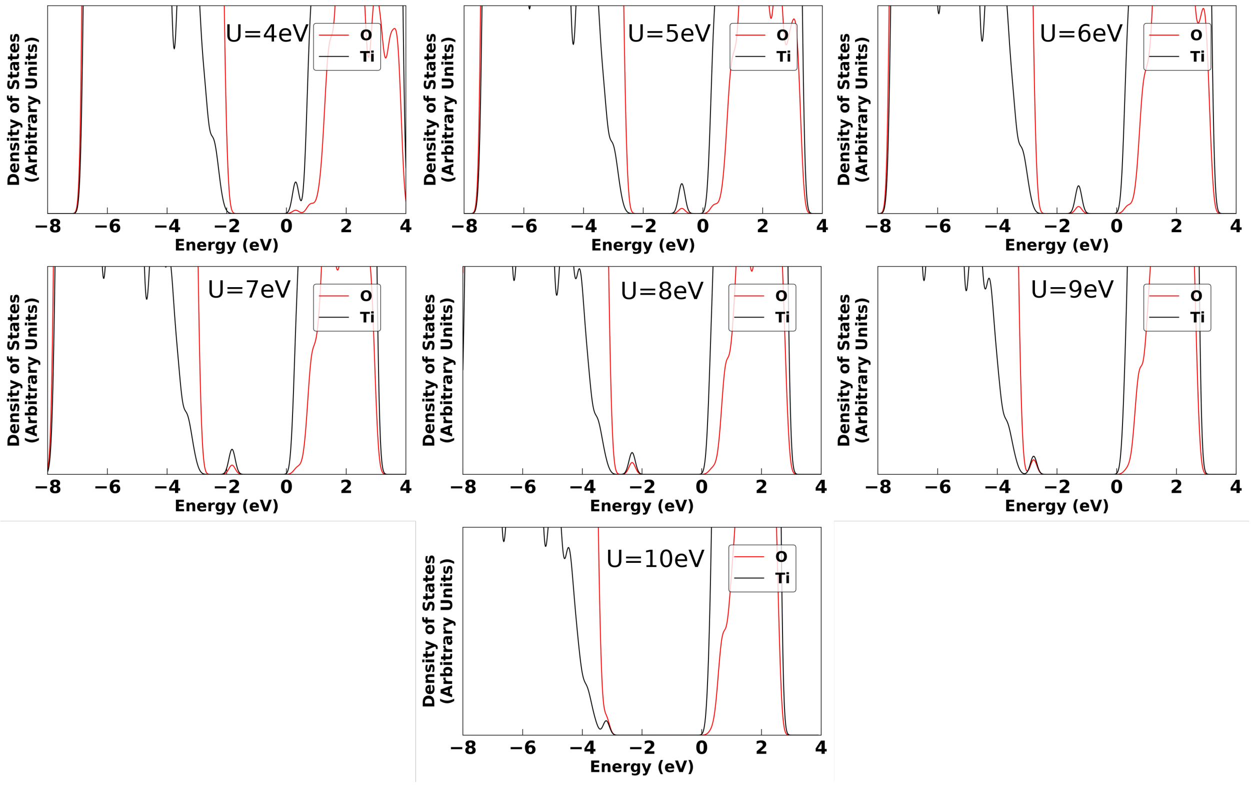

Figure A1: Projected density of states for TiO_2 anatase using different U values where a polaron is formed. The zero energy is chosen as the conduction band minimum (CBM). The polaron exists as a small gap state predominantly on Ti atoms. As U value increasd, the polaron state was shifted from the conduction band to the valence band.

1.2 Electron attractor method

Table A3: Polaron formation energy in eV for TiO_2 anatase at different U(Ti), U(V) and U(Cr) values. A negative value means that a polaron is formed. Non-negative value indicates that no polaron is formed.

	U (Ti) (eV)								
U on substituted atoms	0	1	2	3	4	5	6	7	8
U(V) = 0 eV	0.00	0.00	0.00	0.00	0.00	0.00	-0.83	-1.12	-1.42
U(V) = 4eV	0.00	0.00	0.00	0.00	0.00	0.00	-0.83	-1.12	-1.42
U(V) = 8eV	0.00	0.00	0.00	0.00	0.00	0.00	-0.83	-1.12	-0.66
U(Cr) = 0eV	0.00	0.00	0.00	0.00	0.00	0.00	-0.83	-1.12	-1.28
U(Cr) = 4eV	0.00	0.00	0.00	0.00	-0.13	-0.40	-0.83	-0.98	-1.28
U(Cr) = 8eV	0.00	0.00	0.00	0.00	-0.29	-0.55	-0.69	-0.98	-1.28

Table A4: Polaron formation energy in eV for TiO_2 anatase at different U(Ti), U(V) and U(Cr) values. A negative value means that a polaron is formed. A non-negative value and values with \$ indicated mean that no polaron is formed.

	U (Ti) (eV)								
U on substituted atoms	0	1	2	3	4	5	6	7	8
U(V) = 0 eV	0.00	0.00	0.00	0.00	0.00	0.00	0.00	0.00	-0.34
U(V) = 4eV	0.00	0.00	0.00	0.00	0.00	0.00	0.00	0.00	-1.16
U(V) = 8eV	0.00	0.00	0.00	0.00	0.00	0.00	0.00	-0.84	-1.16
U(Cr) = 4eV	0.00	0.00	0.00	0.00	0.00	0.00	0.00	0.00	$-0.15^{\$}$
U(Cr) = 8eV	0.00	0.00	0.00	0.00	0.00	0.00	0.00	0.00	$-0.08^{\$}$

2 m-HfO$_2$

2.1 Bond distortion method

Table A5: Polaron formation energy in eV for m-HfO$_2$ at different U values and different initial %distortion. A negative value means that a polaron is formed. A non-negative value and value with \$ indicated mean that no polaron is formed.

% Hf-O bond distortion	U$_{effective}$ (eV)										
	0	1	2	3	4	5	6	7	8	9	10
0	0.00	0.00	0.00	0.00	0.00	0.00	0.00	0.00	0.00	0.00	0.00
2	0.00	0.00	0.00	0.00	0.00	-0.04$^{\$}$	-0.06	-0.09	-0.23	-0.39	-0.01$^{\$}$
4	0.00	0.00	0.00	0.00	-0.04$^{\$}$	-0.04$^{\$}$	-0.06	-0.09	-0.23	-0.39	-0.59
6	0.00	0.00	0.00	0.00	-0.03$^{\$}$	-0.04$^{\$}$	-0.06	-0.09	-0.23	-0.39	-0.59
8	0.00	0.00	0.00	0.00	-0.04$^{\$}$	-0.04$^{\$}$	-0.06	0.00	-0.23	-0.39	-0.59

2.2 Electron attractor method

Table A6: Polaron formation energy in eV for m-HfO$_2$ at different U(Hf) and U(Ta) values. A negative value means that a polaron is formed. A non-negative value and values with \$ indicated mean that no polaron is formed.

	U (Hf) (eV)								
U on substituted atoms	0	1	2	3	4	5	6	7	8
U(Ta) = 0eV	0.00	0.00	0.00	0.00	-0.02	-0.04	-0.03	0.01	-0.01
U(Ta) = 4eV	0.00	0.00	0.00	0.00	-0.02	-0.04	-0.03	0.00	-0.01
U(Ta) = 8eV	0.00	0.00	0.00	0.00	-0.02	-0.04	-0.03	0.01	-0.01

3 m-BiVO$_4$

3.1 Bond distortion method

Table A7: Polaron formation energy in eV for m-BiVO$_4$ at different U values and different initial %distortion. A negative value means that a polaron is formed. A non-negative value means that no polaron is formed.

% Hf-O bond distortion	U$_{effective}$ (eV)										
	0	1	2	3	4	5	6	7	8	9	10
0	0.00	0.00	0.00	0.00	0.00	0.00	0.00	0.00	0.00	0.00	0.00
2	0.00	0.00	-0.25	-0.50	-0.77	-1.05	-1.36	-1.68	-2.00	-2.35	-2.70
4	0.00	0.00	-0.25	-0.50	-0.77	-1.05	-1.36	-1.68	-2.00	-2.35	-2.70
6	0.00	0.00	-0.25	-0.50	-0.77	-1.05	-1.36	-1.68	-2.00	-2.35	-2.70
8	0.00	0.00	-0.25	-0.50	-0.77	-1.05	-1.36	-1.68	-2.00	-2.35	-2.70

3.2 Electron attractor method

Table A8: Polaron formation energy in eV for m-BiVO$_4$ at different U(V) and U(Cr) values. A negative value means that a polaron is formed. A non-negative value and values with $ indicated mean that no polaron is formed.

	U (V) (eV)								
U on substituted atoms	0	1	2	3	4	5	6	7	8
U(Cr) = 0eV	0.00	0.00	0.00	0.00	-0.77	-0.47	-1.36	-1.68	-1.51
U(Cr) = 4eV	0.00	0.00	0.00	0.00	-0.77	-1.05	-0.71	-1.68	-2.00
U(Cr) = 8eV	0.00	0.00	0.00	-0.50	-0.77	-1.05	-0.71	-1.68	1.51